


8-2018

POPULATION CODES AND THEIR CORRELATES IN DECISION MAKING

Neda Shahidi

Follow this and additional works at: https://digitalcommons.library.tmc.edu/utgsbs_dissertations

 Part of the [Cognitive Neuroscience Commons](#), [Computational Neuroscience Commons](#), and the [Systems Neuroscience Commons](#)

Recommended Citation

Shahidi, Neda, "POPULATION CODES AND THEIR CORRELATES IN DECISION MAKING" (2018). *UT GSBS Dissertations and Theses (Open Access)*. 888.

https://digitalcommons.library.tmc.edu/utgsbs_dissertations/888

This Dissertation (PhD) is brought to you for free and open access by the Graduate School of Biomedical Sciences at DigitalCommons@TMC. It has been accepted for inclusion in UT GSBS Dissertations and Theses (Open Access) by an authorized administrator of DigitalCommons@TMC. For more information, please contact laurel.sanders@library.tmc.edu.

POPULATION CODES AND THEIR CORRELATES IN DECISION MAKING

A Dissertation Presented

by

NEDA SHAHIDI

Submitted to the Graduate School of the
University of Texas, Health Science Center at Houston
in partial fulfillment
of the requirements for the degree of

DOCTOR OF PHILOSOPHY

June 2018

Neuroscience program

© Copyright by Neda Shahidi 2018

All Rights Reserved

Dedicated to Caro Lucas (1949 – 2010)

who introduced me to the math of the brain

ACKNOWLEDGMENTS

I wouldn't be standing here if I was not lucky to have a great and supportive family. My father, to whom I owe my passion for knowledge and science and the ability to think and reason through problems. My mother, who reminds me every single time that I speak to her, how proud she is of me. My sister, Sara, who is one of my closest friends and makes me laughs through our very long phone conversations, and my sister Narges, the only family member that I had the chance to be around in ups and downs of living far from home.

Speaking of home, I would like to thank all of my friends, especially my Austin friends, who made this city my second home and gave their support, just like a family member. Some people believe that one cannot find new, close friends after a certain age, but my great friends in Austin and Houston proved wrong.

I would like to thank previous and current members of the Dragoi lab who gave me reason to go to work every single day. Ariana Andrei, who is like a sister to me, and is my first go-to person from everything as hard as moving furniture and as fun as painting together; Ming Hu for being my second mentor during the first few years of my PhD; Brian Hansen for his great orientation talk that convinced me to join the lab; Sara Eagleman for teaching me practical tricks of the experiment room; Marcello Mulas, Russell Milton and Sam Debes, my office-mates at different times, for the great chat and snack breaks in the middle of busy days; Adam Jones and Natasha Kharas for being great friends for long discussions about controversial topics; Mircea Chelaru, Ali

Asadollahi and Sunny Nigam for making gatherings and parties more fun; finally, Melissa Franch for keeping the projects alive as I have started to wrap up my work in this lab.

I truly appreciate the department staff, Sharon Gordon, Raquel Cornell, Soraya Thompson, Ismael Perez, Summer Hensley and Amanda Williamson for their hard work to keep the wheels rolling so that we can focus on our study and research. Also, the staff at the animal center, Dr. Julia Goldman, Jessica Grahmann, Cynthia Richmond and Amanda Trimble for providing the best care for our lab animals.

I would like to thank the members of my committee Harel Shouval, Michael Beierlein, Xaq Pitkow, Anthony Wright and Yin Liu for providing detailed feedback to me along the way. Especially Xaq, whose combination of depth of knowledge and great communication taught me a way through the toughest questions of science. I would also like to greatly thank Dr. Dan Felleman for his many pieces of advice and tips on brain anatomy and surgery. I feel lucky to know him and have the chance to learn his techniques.

Finally, I would like to thank Valentin Dragoi, my PhD advisor and mentor, for teaching me, believing in me and supporting me to bring the bests out of my every day's work. His great mentorship skills and strategies provided many opportunities for my growth and prepared me to be an independent researcher. Science is hard, and I know I was not able to overcome the hardship without every day's help of my great mentors.

TABLE OF CONTENTS

	Page
ACKNOWLEDGMENTS	v
AN INTRODUCTION TO POPULATION CODES	10
Population codes	11
Outline of this dissertation	13
PART I NEURAL CORRELATES OF PERCEPTUAL	
ACCURACY	15
CHAPTER I INTRODUCTION AND THE EXPERIMENTAL DESIGN	16
Hypothesis	17
The behavioral task.....	17
Electrophysiological recording of neuronal populations	19
Receptive fields	20
Analysis of single unit activity	21
CHAPTER II DECODING VISUAL INFORMATION FROM THE POPULATION	
ACTIVITY 23	
decoding visual stimuli from spike rates of neurons	24
conclusion	27
CHAPTER III TEMPORAL COORDINATION IN NEURAL POPULATIONS.....	29
Pairwise co-firing and their effectiveness	29
cross-correlation analysis of V1 and V4 neuronal population.....	30
population measures of coordinated spikes.....	32
Higher order coordination within V1 and V4	37
Higher order events across V1 and V4.....	45
Conclusion.....	50

CHAPTER IV	DISCUSSION AND FUTURE DIRECTIONS	53
PART II	STRATEGY ENCODING IN PREFRONTAL CORTEX	59
CHAPTER V	INTRODUCTION TO FORAGING AND OUR EXPERIMENTAL SETUP	60
	The hypothesis.....	62
	The setup of the free-moving foraging task	63
	Variable interval reward scheduling.....	64
	Behavioral training and testing and human interventions	64
	Analysis of the location and the motions of the monkey	65
	Chronic implantation of the Utah array	66
	Recording and Pre-processing the neural activity	67
CHAPTER VI	ANALYSIS OF THE BEHAVIORAL STRATEGY	69
	The analysis of matching behavior for the free-moving foraging task	72
	Determining the foraging strategy and predicting the next action	74
	Summary of results and discussion	77
CHAPTER VII	VALUE CODING AND REWARD EXPECTATION	79
	Decorrelating the neural activity from the task-irrelevant parameters	79
	Decoding Pr_{rew} from the population activity.....	80
	Decoding the K_{loss} from the population activity	83
	Summary of results and Discussion	85
CHAPTER VIII	DISSECTING COMPONENTS OF POPULATION ACTIVITY	86
	Sparse canonical correlation analysis	87
	Results	88
CHAPTER IX	DISCUSSION AND FUTURE DIRECTIONS	92
BIBLIOGRAPHY	94

AN INTRODUCTION TO POPULATION CODES

As many other powerful systems in the nature, the power of the brain emerges from the orchestration of its many elements (Bonabeau, Eric; Dorigo, Marco; Theraulaz 1999). The brain 'divides and conquers' the hardest problems in the world, such as pattern recognition and prediction. Therefore, these processes will not be completely understood without dissecting the processes accomplished by individual neurons, then recombining these neuronal interactions to complete the picture (Anderson 1972). Understanding brain processes in sub-micron resolution is receiving more and more attention around the world as a way of studying human mind and its dysfunctions (Alivisatos et al. 2012; Markram 2006). Moreover, modern computing owes its advances to distributed computing systems inspired by the brain and other biological systems (Patterson 1996). In recent years, a new wave of artificial neural networks, known as deep networks, have solved unique problems in big data analysis (Goodfellow, Bengio, and Courville 2016).

One of the goals of studying the brain is to understand and predict behavior. Classically, behavior is studied using psychology which assumes that the mind is a black box with inputs that are five senses and outputs that are action. In this sense, psychology is using the classical paradigm of control theory in which you study the dynamics of a system's output by finding its relationship to the inputs. As control theory has shifted from the input-output black-box paradigm to understanding components and internal states of a system, the study of behavior has also shifted toward understanding the structure of the brain and the function of its building blocks. Revealing the mechanisms through which the brain controls and shapes behavior would not be possible unless the contributing components and their interactions are studied together.

The precursor to study the population of brain neurons are the tools to record activities of many neurons independently. Simultaneous multi-site recording is continually gaining popularity due to new insights it has brought to information coding.

Population codes

Multiple mechanisms have been proposed to conceptualize how populations of neurons encode information (Figure 0-1):

- Linear rate coding which is basically the weighted sum of neural activity. Essentially, this mechanism assumes that all neurons in the population contribute to a hypothetical latent neuron and each neuron's contribution is proportional to its synaptic weight. Conceptually, the information is represented in a sub-space in the multi-dimensional space of neural activity (Cunningham and Yu 2014; Kobak et al. 2016)(Figure 0-1, left). The subspace might be found using dimension reduction methods (Bishop C.M. 2006).
- Non-linear rate coding takes into account the interaction among the neurons within the population as well (Figure 0-1, right). One result of these interactions is the correlated variability (Averbeck, Latham, and Pouget 2006). The correlated variability was first considered a limiting factor on the information capacity of the network (Zohary, Shadlen, and Newsome 1994). However, later studies showed that correlations can either limit or improve the information coding (Averbeck, Latham, and Pouget 2006).
- Temporal coding takes advantage of the precise timing of the action potential rather than the slow fluctuations in the spike count. In population coding, the relative timing between spikes of pairs of neurons has been measured (Riehle 1997; Vaadia et al. 1995) as a way of inferring the direction of information flow

(Takeuchi et al. 2011b) or the degree to which action potentials converge (Zandvakili and Kohn 2015).

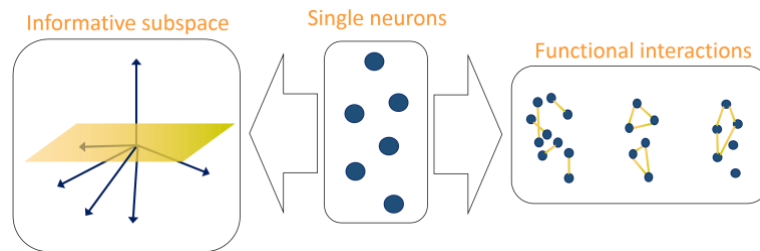


Figure 0-1 Population coding has been studied in two major ways: Finding sub-spaces of the multi-dimensional neural activity that is informative about a particular aspect of external world or internal processes (left) and Estimating the functional connectivity between individual or groups of neurons and its modulation with internal and external processes.

The majority of studies on information coding in cortical populations focus spike rate rather than spike timing. The spike rate codes, at the level of individual neurons or population, examine the modulation of the number of spikes within a window of time that is normally in the range of tens or hundreds of milliseconds. However, this timing resolution is orders of magnitudes coarser than the timing of synaptic computation which is faster than a millisecond. A cortical neuron, for example pyramidal neurons in layer 5 of cortex, is able to detect co-occurrence of incoming spikes that were generated by two different neurons and modulate its output accordingly (Larkum 2013). This phenomenon is an example of temporal integration in cortical populations which would be obsolete if rate coding is the only information coding mechanism in cortex.

From theoretical perspective, a network that is capable of performing temporal coding has higher information capacity compared to a network with rate coding. However, this advantage comes with a cost. The neuronal mechanisms for spike generation and transmission are probabilistic which means that under the same circumstances, a population of neurons does not necessarily generate the same pattern of spikes. Although

this uncertainty affects both spike count and spike timing, the rate coding lowers the variability by average the spike counts over tens of milliseconds. Therefore, rate coding is more robust to noisy variations compared to temporal coding. To summarize, there is a trade-off between information capacity and noise robustness in coding mechanisms (Figure 0-2).

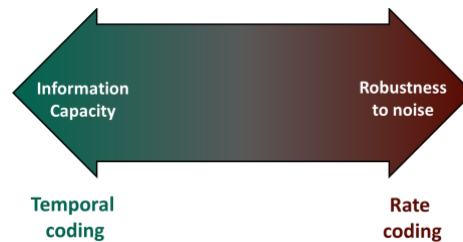


Figure 0-2 Spectrum of information coding. Temporal and rate coding offer distinct advantages that typically come with trade-off: While temporal codes offer more capacity for information coding, the uncertainty of spike timing makes them unreliable. On the other hand, rate coding is robust to noise but requires orders of magnitudes more spikes as well as longer processing time, compared to the temporal coding, to convey the message.

In this dissertation, we explore different coding mechanisms in cortical populations, and their possible roles in perception and decision making.

Outline of this dissertation

PART I: NEURAL CORRELATES OF PERCEPTUAL ACCURACY

The central hypothesis here, is that the spike count codes and spike time coordination play distinct roles in perceptual processing. We provide evidence for this hypothesis in four chapters:

- Chapter I: Approach and experimental setup.
- Chapter II: Decoding visual information from firing rates of population activity.
- Chapter III: The idea of temporal coordination, statistical methods to find temporal coordination, their occurrence in neural population and their role in perception.

- Chapter IV: Summary of the results, alternative hypothesis and possible implications of our hypothesis.

PART II: RULE ENCODING IN PREFRONTAL CORTEX

The central hypothesis here, is that the prefrontal cortical areas construct an internal model of the world to be able to predict the outcomes of one's actions.

We explore this idea in four chapters:

- Chapter V: An introduction to foraging and our novel experimental paradigm.
- Chapter VI: Analysis of the behavioral strategy and prediction of actions
- Chapter VII: Neural correlates of reward expectation
- Chapter VIII: Dissecting the components of the neural activity
- Chapter VIII: Discussion and future directions.

PART I

NEURAL CORRELATES OF PERCEPTUAL ACCURACY

ABSTRACT—The accurate transmission of electrical signals within neocortex is central to sensory perception and cognition. Theoretical studies have long proposed that the temporal coordination of cortical spiking activity controls signal transmission and cognitive function. In reality, whether and how the precise temporal coordination in neuronal populations during wakefulness influences perception remains a mystery. Here, we simultaneously recorded populations of neurons in early and mid-level visual cortex (areas V1 and V4) to discover that the precise temporal coordination between the spikes of three or more neurons carries information about perceptual reports in the absence of firing rate modulation. Perceptual accuracy was correlated with higher-order spiking coordination within V4, but not V1, and with the feedforward coordination between V1 and V4 activity. Our results indicate that while stimulus encoding is related to the discharge rates of neurons, perceptual accuracy is correlated with the precise spiking coordination within visual cortical populations.

CHAPTER I INTRODUCTION AND THE EXPERIMENTAL DESIGN

Perception relies on successive transformations of sensory inputs in the context of local and long-range networks. In primates, which share common pathways of visual processing, the central hypothesis is that cortical processing of visual inputs starts in primary visual cortex (V1) with extraction of fundamental features such as contrast and orientation from the structure of the visual scene. The processing then feeds into midway visual areas, V2-V5 as each area specializes and advances the feature extraction. Although the common belief is that higher order cortical areas are organized into two dorsal and ventral pathways, the extent of common processing and interactions between these areas may show otherwise. However, the evidence that the area V4 in the midway of ventral pathway, is essentially in charge of the static information such as shapes and colors is undoubtable. V4's upstream input is mainly from V2 and its output is to other visual areas in posterior infero-temporal cortex. However, V1 and V4 have reciprocal direct connections as well (Ungerleider et al. 2008). For all mentioned characteristics, V1 and V4 are ideal candidates to study the perception of detailed changes in the natural scenes.

We simultaneously recorded across two visual areas V1 and V4 while monkeys discriminated between natural scenes that were only slightly different. Then, we analyzed the spike patterns of populations to find out where and when the stimulus information was encoded, and what determined the perceptual accuracy.

Hypothesis

We hypothesized that stimulus information is encoded in firing rates while the interactions between neurons affects the accuracy of information transfer between networks of neurons.

Aim1. Decoding the stimulus from activity of population of neurons in each cortical area when the discrimination was performed accurately as well as when the behavioral report was incorrect.

Aim 2. Estimating the strength of interactions within the population of neurons in each cortical area for both cases of the behavioral outcome.

Aim 3. Estimating the strength of interactions between two areas considering reciprocal connections of various time delays.

The behavioral task

We trained monkeys to perform visual discrimination in a delayed-match-to-sample task (Figure I-1). Two monkeys (*Macaca mulatta*) were required to hold fixation within a window with diameter of 1° throughout stimulus presentation. Eye movement was monitored throughout a recording session using an eye tracking system (EyeLink II, SR Research) at a 1 kHz sampling rate. Microsaccades were analyzed using the same method described by (Engbert and Kliegl 2003). Once the animal achieved stable fixation for 200 ms, the target visual stimulus was presented followed by 500-1200 ms of delay period with blank screen and then the test stimulus. Stimuli were presented at parafoveal locations ($4-6^\circ$ eccentricity and away from the vertical/horizontal meridians) and consisted of circular monochromic natural scene with the diameter of $8-10^\circ$. The scene may vary between experimental sessions but were kept the same during a session. The test stimulus was the same as the target stimulus in match trials and was

tilted 3° for monkey C and 5° for monkey W in non-match trials. The orientation difference was selected so that the performance of the monkeys in non-match condition is around 75% (Figure I-2; left). However, the performance of both monkeys on the match trials were higher (Figure I-2; right), compared to the non-match trials which implies that the monkeys might be reporting matching stimuli when they are uncertain about the condition. The fixation was required to be held for 200 ms after the offset of the test stimulus for the trial to be considered valid. After that, the monkeys were cued to respond by changing the color of the fixation point. The correct response was to release the bar for match trials and keep holding it for 1 more second for non-match trials. The response was detected using an impedance detector (Crist instrument response box). If the monkey responded correctly he was rewarded by 5 drops of diluted apple juice automatically (Crist instrument rewarding system). The next trial starts after a 1 second inter-trial time. A total of 200-300 trials were presented during a typical daily session with even numbers of match trials and non-match trials. Stimulus presentation was controlled with custom script using PsychoToolBox. Synchronization between multiple devices (eye tracker, juicer, graphic card) was controlled by the Experimental Control Module (ECM, FHC, Inc.) to ensure the best timing accuracy.

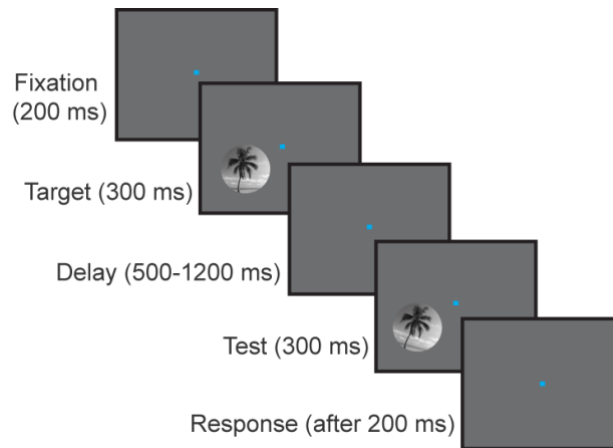


Figure I-1 Delayed match to sample image discrimination task using natural scenes as the visual stimuli. Animals were trained to report whether two briefly flashed successive natural scenes (target and test) were identical or different.

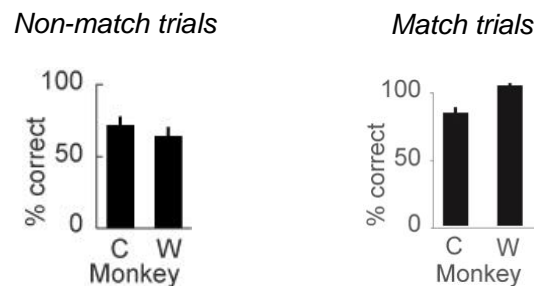


Figure I-2 Behavioral performance of two animals – monkey W: 60 ± 5% correct responses in non-match trials and 90±2% in match trials; monkey C: 73 ± 7% correct responses in non-match trials and 85±4% in match trials.

Electrophysiological recording of neuronal populations

Visual cortex areas V1 and V4 were simultaneously recorded extracellularly using laminar probes (16 channels Plexon U-probe, Figure I-3), similar to previous experiments done in the lab (Hansen and Dragoi 2011). Neuronal and behavioral events were recorded using the Plexon system (Plexon, Inc.). Real-time neuronal signals were amplified, recorded, and stored with Multichannel Acquisition Processor system (MAP, Plexon, Inc.) at a sampling rate of 40 kHz and stored digitally. Neuronal spikes were first identified by visual inspection in a virtual oscilloscope and heard through a speaker.

Spike waveforms that crossed a user-specified threshold voltage [typically 4 standard deviations (SD) of the baseline] were automatically separated from the raw waveform and stored for further offline analyses. The spike waveforms were sorted using Plexon's offline sorter program (using waveform clustering based on parameters such as principle component analysis, spike amplitude, timing, width, valley, and peak).

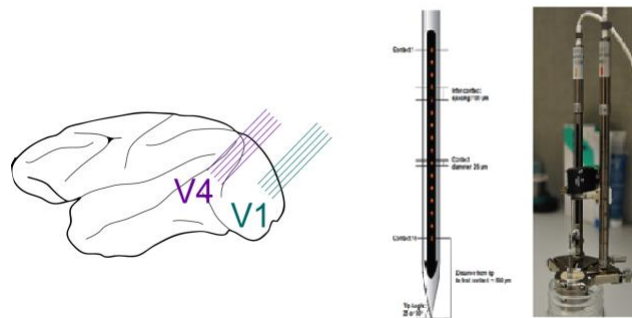


Figure I-3 Electro-physiological setup for simultaneous recording from population of neurons in V1 and V4. Each area may contain 1 or more U-probes, each with 16 channels. The U-probes has been inserted into the brain tissue using electronically controlled advancement equipment (picture in the panel on the right).

We analyzed the spiking activity of 293 single neurons (up to 14 cells per area in each session) that were significantly modulated by the stimuli used in our experiments (at least a 4-fold response increase with respect to baseline).

Receptive fields

Both stimuli fully covered the receptive fields of the neurons recorded simultaneously in each session (there was an 80% overlap between the receptive fields of the cells recorded in V1 and V4; Figure I-4).

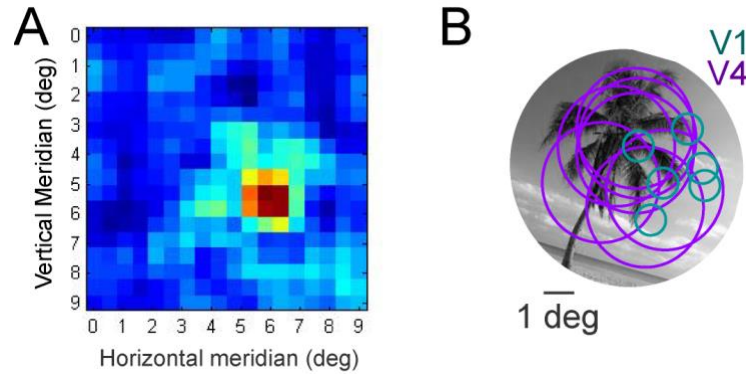


Figure I-4 A) The receptive field of a sample neuron represented as orange and red pixels within the lower left quadrant of the visual field (other quadrants are not shown) B) Receptive field positions of individual V1 (green circles) and V4 neurons (magenta circles) recorded simultaneously in a representative session are shown with reference to the visual stimulus.

Analysis of single unit activity

Sorted spikes were further analyzed for firing rates for the time course of the trial for which fixation was stable (200 ms before the target stimulus and 200 ms after the test stimulus). The PSTHs of spikes were generated by averaging the spike trains binned at 1 ms for the time course of the trial. A spike train was accepted as a visually responsive neuron if the firing rates during the target and test stimuli were greater than 4 SD of the firing rates of the baseline period (200 ms before the target stimulus; Figure I-5A). Typically, neurons show both transient and sustained responses to stimuli and the response may vary with the orientation of the natural scene (Figure I-5B).

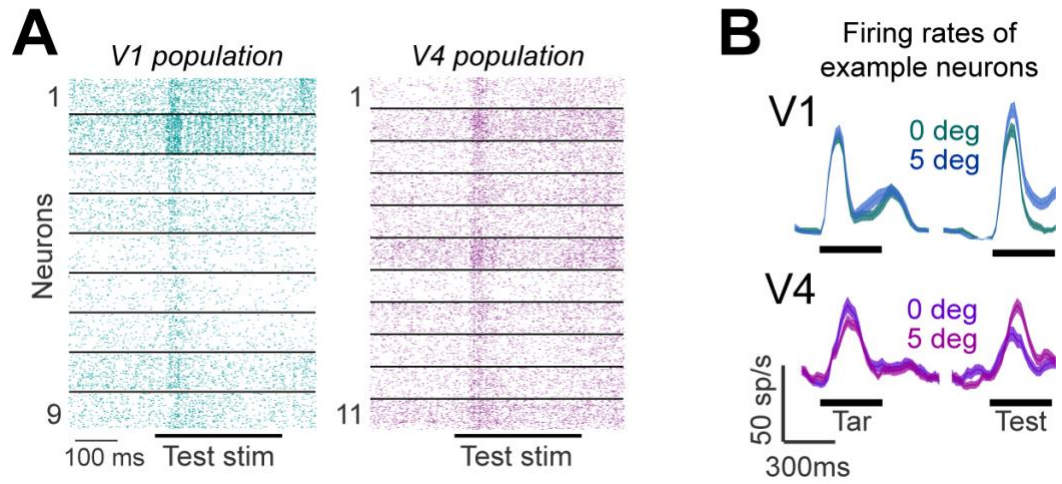


Figure I-5 **A)** Raster plots of spiking activity of simultaneously recorded neurons in V1 and V4. The horizontal bar represents the time of test stimulus presentation. **B)** Sample histograms of spike rates for the target and the test stimuli separated for trials with 0 and 5° test stimuli.

CHAPTER II **DECODING VISUAL INFORMATION FROM THE POPULATION ACTIVITY**

Inferring information coding from differences in neural activity that are averaged across trials of the same condition is a common practice in neuroscience. However, trial averaging is not the brain's way of separating signal from noise. Moreover, individual neurons respond diversely, when encoding information. Therefore, a trial average analysis might not be conclusive about the role of each neuron in information coding at any time. Recently, the trial by trial decoding analysis has gained popularity in the field. The idea is to train a decoder to classify experimental conditions based on the activity of individual neurons or their populations. To compare two specific experimental conditions, a wide range of binary classifiers have been used.

In our orientation discrimination experiment, we are interested to know if neural firing rates are informative about the orientation of the visual scene. The test stimulus appears in two conditions: match and non-match, with 3-5 orientation differences. The trial average firing rates in these two conditions were different for some neurons. However, to demonstrate that the information about the visual stimulus condition was encoded in the neural population, we used a class of standard decoders, called Support Vector Machines (SVM), to decode the condition from the population activity within recorded brain areas. SVM classifiers essentially find a hyperplane in the reduced dimension space with the shape of the defined kernel function; however, they use support vectors to place the hyperplane within the gap between the two conditions optimally to allow the best generalization. The classifier's performance is measured by the percentage of trials that were classified correctly. However, to avoid over-fitting, the classifier was trained

and tested using a segregated set of trials. When only one set of trials is provided, this can be accomplished by randomly dividing the set to non-overlapping training and test sets for a number of iterations. This procedure is called cross-validation.

To determine the statistical significance of the classifier's performance, the distribution of the values (across cross-validation iterations, different sessions, etc.) may be tested against the chance level. Sometimes the chance level is not at 50% because the classifier is biased toward one of the conditions. For example, when the number of trials for two conditions are highly imbalanced (e.g. 80% class 1 and 20% class 2) a trivial classifier that classifies everything as class 1 tends to be 80% correct on average. To determine the chance level for this classifier, the cross-validation may be repeated on the data with shuffled class labels. In the case of trivial classifier, the shuffled classifier performs 80% correct as well, which means the original data was not classified better than the chance level.

DECODING VISUAL STIMULI FROM SPIKE RATES OF NEURONS

To determine if the neural populations in V1 and V4 are able to discriminate between the two images (rotated or not), we trained classifiers using the firing rates of simultaneously recorded neurons. We used support vector machines to determine if stimulus is encoded in firing rates of V1 or V4 populations. The parameter of a linear kernel function was tuned to the training data. The decoder performance was determined as the percentage of correctly classified test samples. The training and test trial sets are determined based on the purpose of decoding. When cross-validation was done, the trials were randomly divided to training (80%) and test (20%) subsets for 1000 iterations, the performance of the decoder was assessed in each iteration and the average over iterations of the performance was used. The shuffled decoders were trained and tested on data with

randomly shuffled class labels. Performance of shuffled decoder was used as a null hypothesis for statistical testing the decoder performance. As an additional control, the decoders were trained and tested using sliding window on spiking data, starting before the presentation of the test stimulus, when decoding the upcoming test stimulus is logically impossible.

Using SVM classifiers to decode V1 and V4 populations, Both areas were able to decode stimulus orientation in 'correct' trials significantly above chance level determined by shuffling across correct and incorrect trials (Figure II-1; p-value of Wilcoxon signed rank test was smaller than 0.01 for any 200 ms window in V1 that was overlapping the stimulus presentation time or any window in V4 starting 200 ms after test onset). However, in incorrect trials we found that stimulus orientation is only encoded correctly by the V1, but not the V4, population (Figure II-2, p-value of Wilcoxon signed rank test was smaller than 0.05 as early as 100 ms after test onset in V1, but always bigger than 0.2 for any window in V4). That is, despite the fact that firing rates of neurons were not significantly different between correct and incorrect trials (p-value of Wilcoxon sign rank test was 0.51 for V1 and 0.79 for V4), the task relevant information required for a correct behavioral report was only present in V1, but not V4.

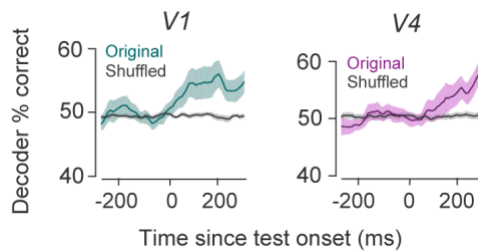


Figure II-1 Decoding the stimulus in correct trials. Performance of a classifier that uses firing rates of all simultaneously recorded neurons in V1 and V4 to decode the test stimulus (we used a 200 ms window sliding in 20 ms increments). The classifier was trained using 80% of all correct trials and performance validated by classifying the remaining 20% of trials (performance was cross-validated 1000 times by randomly dividing trials to training and test sets). Shuffled classifier – trial labels (stim 1 vs. stim 2) were shuffled before training and then the cross-validation procedure was repeated. The results in the figure belong to SVM with linear kernel but the results with quadratic as well as RBF kernels were very similar.

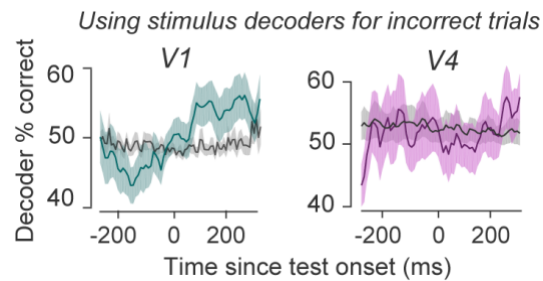


Figure II-2 Decoding the stimulus in incorrect trials. The classifiers were trained using all correct trials, then tested on incorrect. The rest of the procedure is similar to the previous figure.

Results of the decoders, show that the performance of the decoder is higher than the chance level for V1 which suggests that perceptual inaccuracy occurs in downstream areas. However, in V4, the decoder's performance is about the chance level suggesting that the information about the identity of the stimulus is missing in this area. Given that the primary flow of the visual information is feedforward, the lack of information in V4, but not V1, suggest that the information was lost either in the areas between V1 and V4 or within V4.

To further examine the role of each area in perceptual processing we examined the correlation of firing rates within each population with the behavioral outcomes using SVM decoders. To classify correct and incorrect trials using SVM decoders, we trained the decoder using the firing rates of V1 or V4 population within a 200 ms sliding window, similar to the stimulus classifiers on the previous section. None of the visual areas were able to decode the behavioral outcome better than the chance level (Figure II-3).

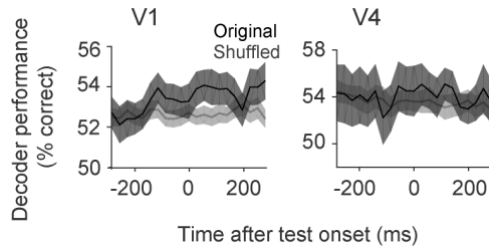


Figure II-3 Performance of the classifier that uses the firing rates of all simultaneously recorded neurons to decode perceptual accuracy (correct vs. incorrect reports). A 200 ms window sliding in 20 ms incremental steps was used. The classifier was trained using 80% of the trials and performance was measured by classifying the remaining 20% of trials. The performance was cross-validated 1,000 times by randomly dividing trials to training and test sets. In shuffled classifiers, the trial labels (correct vs. incorrect) were shuffled before training; then the cross-validation procedure was repeated. The performance of the classifier was not significantly different from the null hypothesis ($p > 0.1$, Wilcoxon signed tank test) for any analysis window in any cortical area.

CONCLUSION

In this chapter, we asked whether the information about the visual stimuli that is relevant to our orientation discrimination task are encoded in visual areas V1 and V4. We found that when monkeys report the presented stimulus correctly, we are able to decode the stimuli from population of neurons in either V1 or V4. When the behavioral report was incorrect, we used the trained decoder to determine if either the presented or the reported stimulus is encoded in each area. We were able to decode the presented stimulus from V1 activity. However, neither the presented nor the reported stimulus was decoded from V4. Our further attempt to decode the behavioral reports from V1 or V4 population activity failed as well. We conclude that firing rates of neurons in V1 is encoding the visual stimulus, regardless of perceptual accuracy. However, when perception is inaccurate, V4 activity is missing the information on the identity of the stimulus. We hypothesize that loss of stimulus information in V4 or in the feedforward pathway between V1 and V4 is responsible for the inaccuracy of perception. Because the majority of the incorrect trials were non-match conditions which were reported as match by the animal, we speculate that, in the absence of information, monkeys go with their default response (which is reporting a match due to the discussion in the previous chapter on Figure I-2). The

relative spike timing between neurons in the same network is suggested to modulate the efficacy of synaptic connections between them in previous studies. Therefore, we examined the relative timing of spikes in the following chapter.

CHAPTER III TEMPORAL COORDINATION IN NEURAL POPULATIONS

Temporal dependency of spike events has been considered a measure of functional connectivity between neurons when direct examination or causal manipulation is not possible. Given the complexity of connectivity pattern in cortical networks as well as the uncertainty of synaptic connections, the chance that every single spike of a neuron is time-locked to one or more spikes of its network neighbors is very small. Therefore, methods to detect coordinated spikes are optimized to detect rare events that occur beyond the chance level.

PAIRWISE CO-FIRING AND THEIR EFFECTIVENESS

Cross-correlogram is an established method to detect correlation of spike timing and spike count (Alonso, Usrey, and Reid 1996; Alonso and Martinez 1998; Cohen and Kohn 2011; Takeuchi et al. 2011b)(Figure III-1).

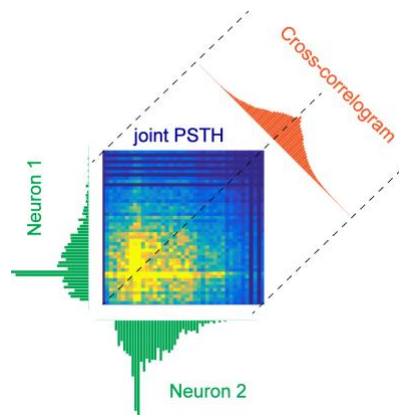


Figure III-1 jPSTH and cross-correlogram. jPSTH shows the histogram of time bins across trials with co-occurrence of spikes of both neurons in the pair. While marginal histograms along each access are PSTH of each neuron, the marginal histogram along the unity line is the trial averaged cross-correlogram of the pair.

Normally the magnitude of cross-correlogram peak indicates the proportion of the spikes that are shared between two neurons and the shape of the peak as well as its deviation from the center helps identifying the source of the shared spikes (Figure III-2).

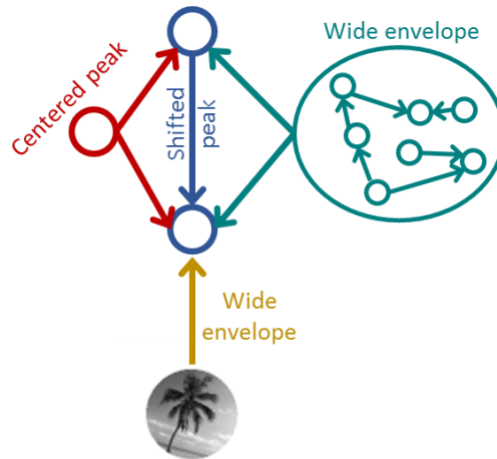


Figure III-2 types of CCG peaks. A common input that is one or a few synapses away produces spikes with precise timing (± 10 ms) which will appear as a sharp peak. If the time of arriving to each post-synaptic neuron is different, the peak would be shifted. This case might not be distinguishable from the case that the two neurons are connected themselves for which a shifted sharp peak will be observed as well. If the source of common input is many synapses away (such as a visual stimulus within the receptive fields of both neurons or common input from other areas of the brain) the peak will be wide due to inconsistency of the timing of evoked spikes.

CROSS-CORRELATION ANALYSIS OF V1 AND V4 NEURONAL POPULATION

We applied cross correlation method to all possible pairs of simultaneously recorded V1 or V4 neurons as well as cross area pairs in V1 and V4. The trial average of spike trains binned to 1 ms were able to capture the precise temporal dynamics of firing rate modulation while the Instantaneous firing rate (IFR) was able to capture the slow dynamics of this modulation (Figure III-3). When Cross-correlogram (CCG) of the spike trains as well as CCG of the IFRs were calculated, the CCG of IFR was able to capture the bell shape envelop of the raw CCG.

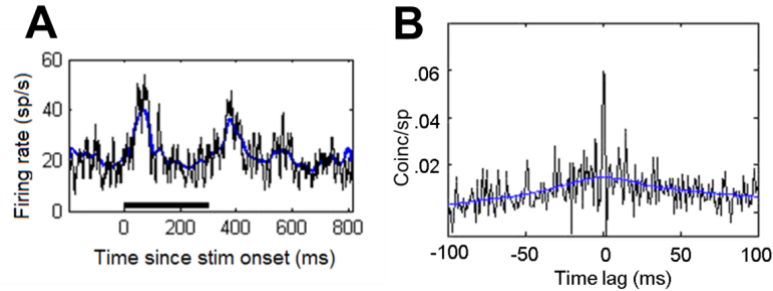


Figure III-3 IFR correction. A) The trial averaged firing rate (black) for a sample neuron and the IFR (blue) which is the trial average of inverse of the inter-spike time. B) Cross-correlation of spike trains for a sample pair (black) overlapped with the cross-correlation of their IFR traces (blue).

We calculated IFR corrected CCGs for all correctly reported trials of the match stimulus as well as all trials of the non-match stimulus. Then for each stimulus-behavior category, we examined the statistical significance of the trial averaged CCG peak by comparing it to confidence interval of the tail as explained in the previous sub-chapter. To determine if the visual stimulus is reflected in the functional connectivity of pairs of neurons we compared trial average CCG of match-correct to non-match correct. Figure III-4A shows an example pair in each cortical area for which the peak of CCG is slightly different for two visual stimuli. We identified all such pairs with a significant peak (bigger than 95% confidence interval of the tail) and averaged the area under the peak within ± 10 ms range of the time lag across all significant peaks within the same session. Across all our sessions (Figure III-4B), the area under the peak does not show a strong tendency toward either match (stim1) or non-match (stim2) condition ($p > 0.085$ for V1 and $p > 0.67$ for V4, Wilcoxon signed rank test across sessions).

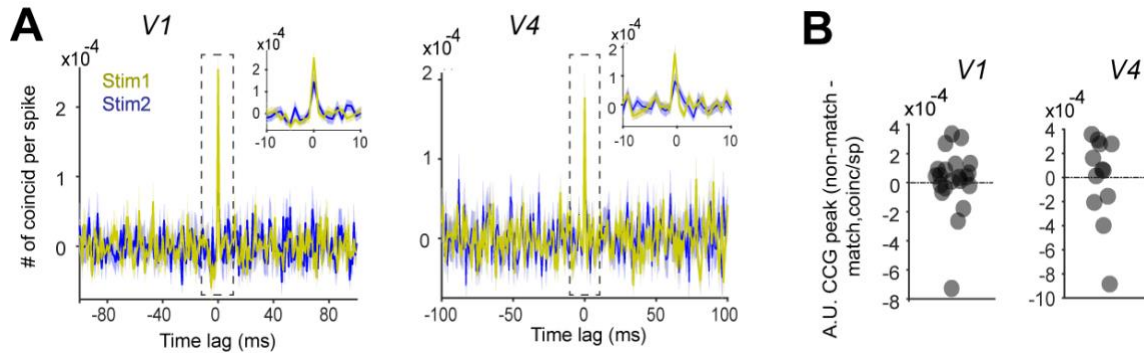


Figure III-4 Cross correlogram analysis of two conditions with different visual stimuli. **A)** The cross correlation of all pairs in V1 (left) and V4 (right) areas separated averaged over trials with stim1 and stim2 test stimuli. Insets: Magnified peak that were indicated with dashed lines in the main panels. **B)** The difference between the area under peak for cross-correlation of the two stimuli. Each point represents the average difference for one session.

Similarly, we compared the cross-correlograms of non-match correct trials to that of the non-match incorrect. Although for some pairs, the peak of CCG shows slight difference between correct and incorrect trials (Figure III-5A) we did not observe any significant difference between two conditions across all sessions (Figure III-5; $p > 0.27$ for V1 and $p > 0.79$ for V4, Wilcoxon signed rank test across sessions).

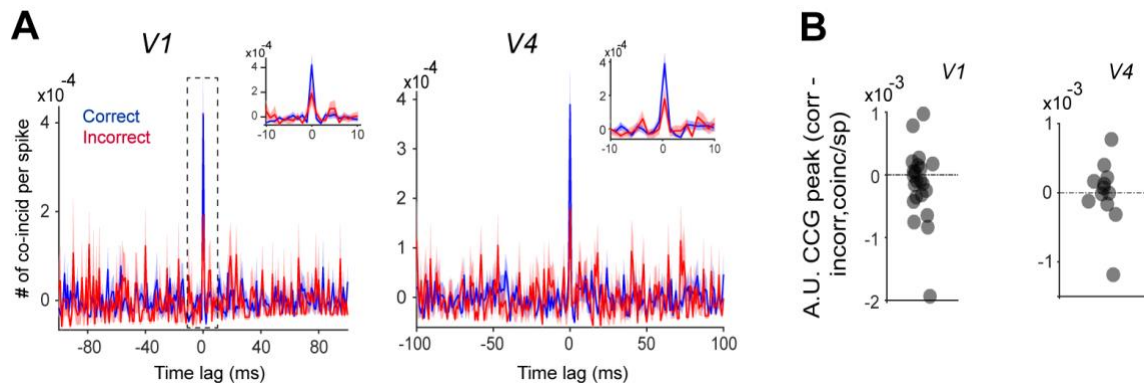


Figure III-5 Cross correlogram analysis of two conditions with different behavioral outcome. **A)** The cross correlation of all pairs in V1 (left) and V4 (right) areas separated averaged over trials with correct and incorrect trials. Insets: Magnified peak that were indicated with dashed lines in the main panels. **B)** The difference between the area under peak for cross-correlation of the two behavioral outcomes. Each point represents the average difference for one session.

POPULATION MEASURES OF COORDINATED SPIKES

Extending the idea of pair-wise correlations to the population of three or more neurons is not trivial due to exponentially increasing complexity of interactions. Methods for

assessing coordination and synchrony in simultaneously recorded populations relies on state of the art statistical models and hypothesis testing (Aertsen et al. 1989; Pipa et al. 2008; Torre et al. 2016, 2013; Riehle 1997). Here we modified and used a simple, yet statistically powerful tool called NeuroXidence to find coordinated assemblies of neurons within a population.

The frequencies of occurrences of coordinated events were empirically estimated using NeuroXidence tool available as Matlab code in <http://www.ni.uni-osnabrueck.de/~ni/www.neuroxidence.com/>. The essence of the method is to find the time bins (5 ms) containing a certain pattern p which consists spikes from certain neurons. For example, the pattern

$$p_i = x1xx1xxxx1$$

contains spikes from 2nd, 5th and 10th neurons in a set of 10 neurons. The other neurons may or may not have a spike in this pattern (x for either 0 or 1). Confounding factors (such as binning, multiple spikes from the same neuron within the same time bin, co-fluctuation of firing rate) were corrected using the jittering method detailed in (Pipa et al. 2008). For n neurons, the number of patterns N presenting a co-firing of 2 to n neurons is

$$N = 2^n - n - 1$$

For each of the N patterns the coordination rates F for a time window of length t sec in trial j were calculated as

$$F_j^{p_i} = \frac{\text{number of bins showing pattern } p_i}{t}, i = 1, \dots, N$$

To determine if a pattern is occurring significantly higher than chance, the frequencies of occurrences of this pattern across a set of trials were tested against a null hypothesis

which is the frequency of occurrences of the same pattern in jittered spike trains. Essentially, jittering is shifting each spike train in time relative to the other spike trains (Figure III-6-right). Jittering must be performed in a time scale shorter than the time scale of possible co-fluctuations of firing rates and longer than a single time bin (± 10 ms; Figure III-6).

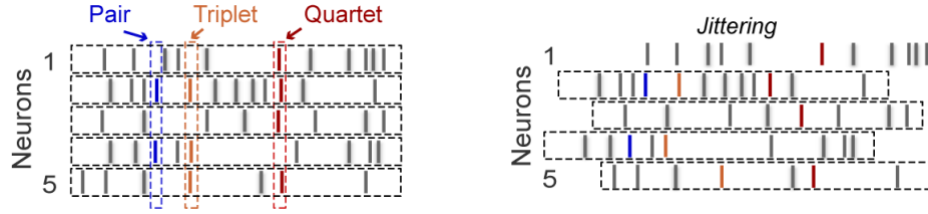


Figure III-6 Cartoon showing coordinated spike events in groups of 2 or more neurons. Sample pair (blue), triplet (orange) and quartet (red) coordination are shown. Coordination rates in jittered spike trains (bottom) were used as null hypothesis to determine the statistical significance of coordinated spiking.

The jitter corrected frequencies of occurrences were calculated as

$$\Delta F_j^{pi} = F_{j,original}^{pi} - F_{j,null}^{pi}$$

Which were tested for significance using Wilcoxon signed rank test. When compared between two trial sets (such as correct vs. incorrect or match vs. non-match) all patterns occurring at a significant rate ($p < 0.01$) within either of trial sets were selected for analysis. An exception was the raster plot in Fig. 3A for which we had to exclude the patterns for which the rate of occurrence is not significantly different between correct and incorrect trials (Wilcoxon signed rank test, $p > 0.01$) to optimize the visibility. The total frequency of occurrences for all patterns of size c (patterns that include spikes from at least c neurons) in correct trials was calculated as

$$F_{corr}^c = \sum_{p \in signif} \sum_{j \in corr} \frac{\Delta F_j^p}{N_{corr} \times N_c}, c = 2, 3, \dots, N$$

in which N_{corr} is the number of correct trials and N_c is the number of size c patterns regardless of significance which, for a sizable population, is growing rapidly with c for $c=2,3$ and 4 (Figure III-7).

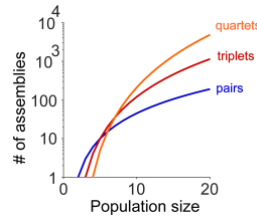


Figure III-7 Number of patterns as a function of population size. The patterns of size 2 (pairs), size 3 (triplets) and size 4 (quartets) are shown.

The frequencies of occurrences for incorrect trials and match correct trials were calculated similarly. To avoid the effect of unbalanced sets of trials on test power, bootstrapped distributions were generated as below: the trial sets were resampled with replacement (sample size was 100), then p-value of Wilcoxon signed rank test was calculated for each sample set. The procedure was repeated to obtain a distribution of p-values from which the mean p-value was compared to the threshold which was 0.01.

One major concern around this method is the false identification of coordinated spikes when the firing rates co-fluctuate due to firing rate modulation to stimulus and other non-stationary events. Therefore, we simulated spikes with the exact same statistics as our recorded neurons and computed the coordination rates while varying the co-fluctuations of spike counts. To generate independent spike trains with the same statistics of the real neurons, first we generated spikes for each neuron using a Poisson processes for which the rate of events at any 1 ms time bin was the trial averaged firing rate of the actual neuron. To generate spike trains with, say 20% shared spikes among neurons, first we generated independent spike trains so that the firing rates are 20% lower than the actual firing rates, then added the shared spikes across the entire population, to match the

spike count of the actual neurons, but with random timing within a 50ms window (Figure III-8).

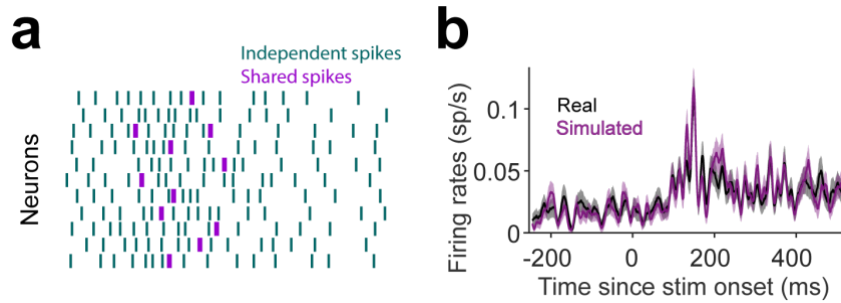


Figure III-8 Simulation of spike trains with similar statistics to our actual neurons. A) spike trains that are generated using independent Poisson processes (green) as well as spikes that are shared among the population to increase the spike count correlation without increasing the spike-time correlations. B) Trial-averaged histogram of spike counts for 200ms before to 500 after the time of stimulus onset for an actual neuron as well as simulated neuron.

This method does not add any coordinated spikes to the population and we know this because the cross-correlograms of the spike trains do not show any sharp peaks (Figure III-9a). However, the spike count correlation increases monotonically with the percentage of shared spikes (Figure III-9b).

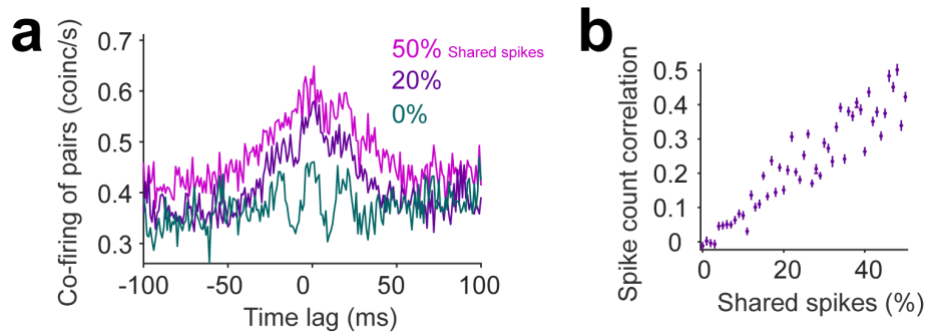


Figure III-9 Relationship between the percentage of shared spikes and the spike time and spike count correlations. A) cross-correlogram averaged across trials as well as all pairs within the population for various percentages of shared spikes. B) Pearson correlation coefficient of spike counts across trials averaged for all pairs within the simulated population as a function of percentage of shared spikes.

The coordination rates for the simulated population is not expected to be better than the chance level. We calculated the coordination rates combined across all pair-wise and higher order assemblies of neurons within this population, then applied jitter correction, we observed that the coordination rates for 0-50% shared spikes, which translates to

spike count correlation of 0-0.5. We observed less than 0.002 coordinated events per second which was 50 times smaller than coordination rates in the actual population which was around 0.1 coordinated events per second (Figure III-10).

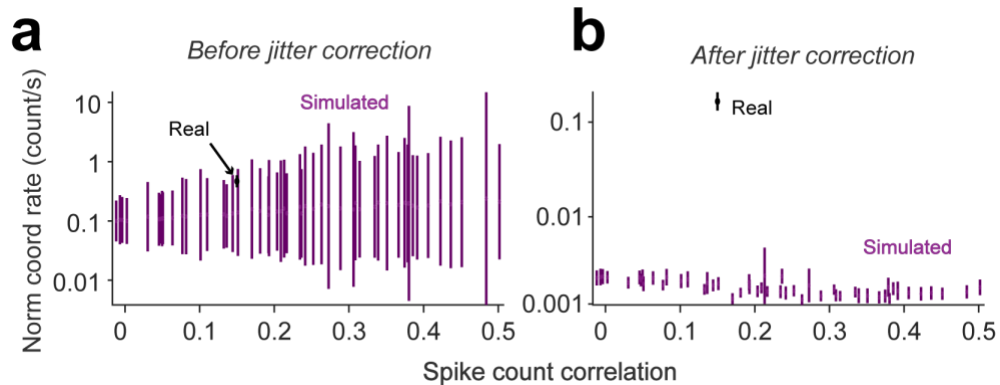


Figure III-10 Coordination rates for all simulated populations as well as the real population. A) coordinated rates averaged for all assemblies of neurons (size 2 to 12) regardless of the significance of their occurrence. B) Coordination rates of panel 'a' after subtracting the coordination rates of surrogate data that was generated by jittering the spike trains (jitter range= 10ms).

In the rest of this chapter, we present our findings with coordination rate analysis of V1 and V4 populations.

HIGHER ORDER COORDINATION WITHIN V1 AND V4

We detected coordinated spiking in simultaneously recorded neuronal populations by calculating the frequency of near-coincident (5 ms) firing of two or more neurons on a trial-by-trial basis that occurred significantly more often than expected by chance. The coordination rate was calculated by dividing the number of coordinated event occurrences by the time length of the analysis window. The statistical significance of coordination rates was tested against the null hypothesis generated by jittering the spike trains (jitter range was ± 10 ms; 20 jittering iterations). Jittering spike trains preserves all statistics including periodic oscillations, co-fluctuations of firing rates and trial by trial

variability but not the precise timing of spikes. Therefore, subtracting coordination rates of jittered spike trains from that of the original spike trains before testing for statistical significance alleviate the possibility that significantly detected coordination rates may be due to coherent oscillations or co-fluctuations of firing rates (Pipa et al. 2008b) We interpreted a coordinated spike event as representative for the subset of neurons that were engaged in a cell assembly at a given time. Note that we refer to cell assemblies of size 3 or above as higher-order coordination which is different from higher order models used for reconstructing spike trains (Schneidman et al. 2006; Ganmor et al. 2011; Ohiorhenuan et al. 2010).

We calculated coordination rates around the time of the stimulus presentation and observed that that coordination between 2, 3, and 4 spikes is not a random event, but is frequently encountered during the stimulus-evoked response (Figure III-11).

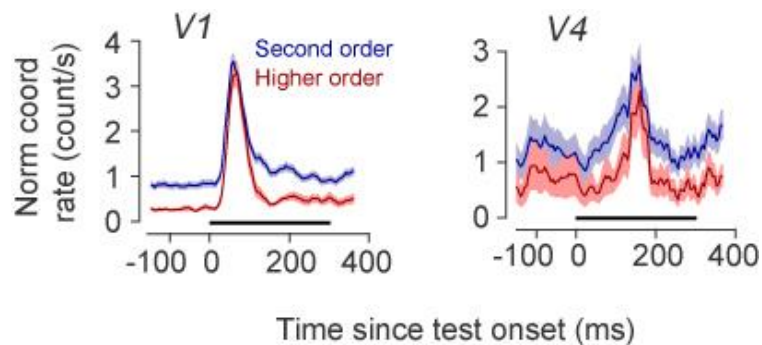


Figure III-11 Normalized rate of occurrence for second order (pairs) and higher order (triplets and above) significantly occurring coordinated events within a 300 ms stimulus window shifted in 20 ms increments (average of 22 V1 and 12 V4 sessions).

However, there was no relationship between stimulus orientation and coordination rates in V1 or V4 for any size of the neural assemble (Figure III-12, left). We further used ROC analysis to examine the relationship between coordinated events and the orientation of the test stimulus. The area under the ROC curve is typically used to determine the

performance of a binary classifier discriminating between two conditions. When the area under ROC is different from 0.5, the classifier's performance is better than chance level. As shown in Figure III-12-right, insets, the area under ROC curve for coordination rates of various sizes is not significantly different from 0.5 (Wilcoxon signed rank test, $p > 0.1$ for all comparisons; Figure III-12, right) in either V1 or V4, which indicates that stimulus encoding is unrelated to the precise temporal coordination of neuronal spiking. These results are consistent with the long-standing idea that stimulus-specific information is transmitted in the neocortex by firing rate modulations, not by the precise spike coordination².

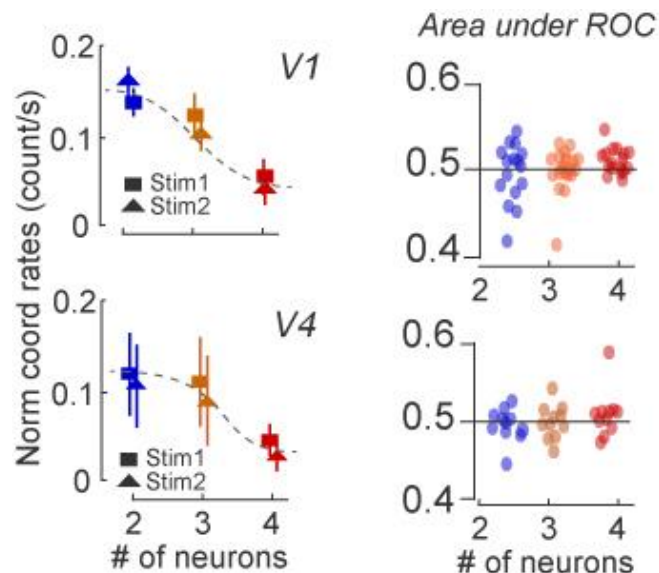


Figure III-12 Coordination rates in V1 and V4 during the presentation of each test stimulus (stim1 and stim2) as a function of ensemble size. Inset: area under ROC curve for stim1 and stim2 trials averaged across coordinated events of order 2 (blue), 3 (orange) and 4 (red) shown for each session. Each data point represents one session.

We further tested whether the spiking coordination rate, as a measure of effective neuronal communication, is correlated with behavioral outcomes. To this end, the correct and incorrect responses in each session were separated to investigate the correlation between coordinated spiking rate and the behavioral choice. The example session in

Figure III-13 shows the responses of nine V1 neurons and twelve V4 neurons for 42 correct and 42 incorrect trials. Coordinated spikes for pairs of cells and higher order assemblies (order 3 and more) were color coded. This panel only shows a subset of significantly occurring coordinated spikes for which the coordination rates were different between correct and incorrect conditions (Wilcoxon rank sum test, $p < 0.01$), however other significantly occurring events were also included for the analysis.

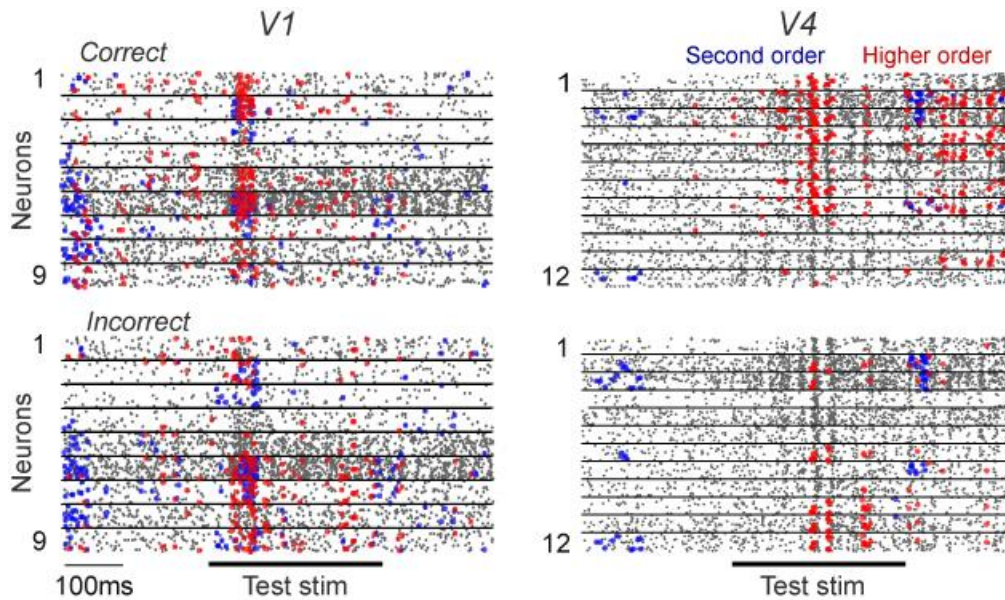


Figure III-13 Raster plots of nine V1 and twelve V4 cells from a single session for correct and incorrect trials. Overlaid are combinations of 2 (blue) or more (red) spiking coordinated events, subsampled for clarity with an equal number of randomly selected trials showing patterns for which the frequency of occurrence is significantly different between correct and incorrect sets ($p < 0.01$, Wilcoxon rank sum). The horizontal lines mark the presentation of the test stimulus.

To quantify this effect, we calculated the frequency of occurrences of coordination rates. It is apparent from Figure III-14 that whereas pairwise coordinated events in V1 and V4 were unrelated to behavioral outcomes, there was a clear increase in the frequency of higher-order spiking events for correct trials predominantly in area V4. In contrast, neuronal coordination in V1 did not appear to be related to behavioral decisions.

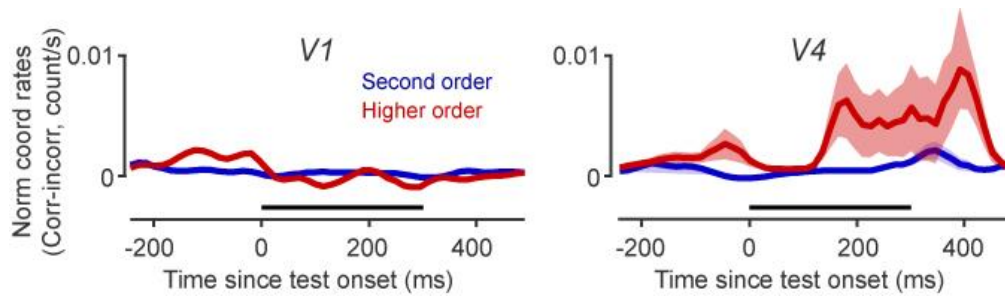


Figure III-14 The normalized coordination rates in V1 and V4 represent the difference in the frequency of occurrences of coordinated events (correct – incorrect) represented in panel d, calculated for a 300-ms window sliding every 10-ms.

The relationship between the coordination rate in higher-order ensembles and behavioral decisions was a general phenomenon across our recording sessions in both animals. We analyzed our population of recording sessions ($n=22$ in V1, and $n=12$ in V4) using a 300-ms sliding window with a 10-ms step (Figure III-15). The analysis included only the coordinated spiking events that were statistically significant (Wilcoxon signed rank, $p<0.01$) in either correct or incorrect trials regardless of the assemble size. For pairs of neurons, the difference in coordination rates was highly variable but not statistically significant for any time window, both in V1 and V4 populations ($p>0.1$, Wilcoxon signed rank). In contrast, the triplets and quartets in V4 carried significant information about behavioral decisions following test stimulus onset ($p<0.05$, Wilcoxon signed ranked test). For all other times shown in Figure III-15 the difference in coordination rates were not significant ($p>0.1$, Wilcoxon signed rank). We restricted this analysis to neuronal ensembles of size 4 and below; although we identified coordinated events for ensembles of order 5 and above, they were only found in a limited number of sessions, and their frequency of occurrence was insufficient to assess statistical significance.

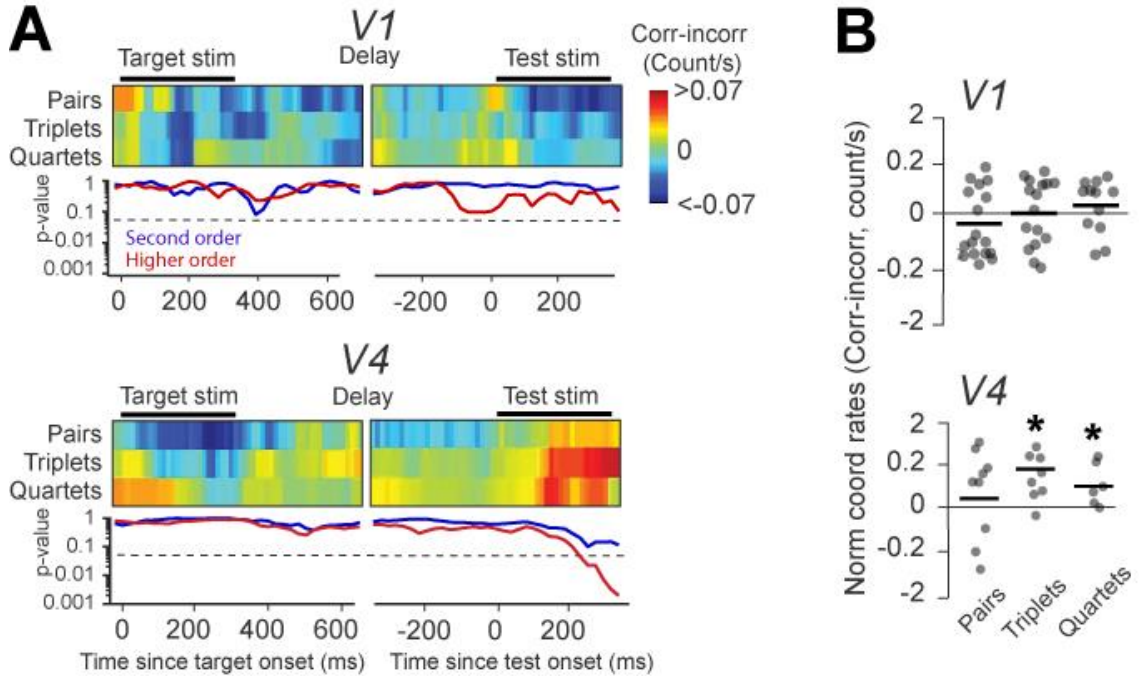


Figure III-15 (A) Top panels: The difference in coordination rates (for pairs, triplets, and quartets) between correct and incorrect trials measured using a 300-ms window shifted in 10-ms increments (average of 22 sessions in V1 and 12 sessions in V4). The small gap during the delay period is due to the variable interval between target and test. Bottom panels: Statistical significance of the Wilcoxon signed rank test (P-value) for the difference in coordination rates between correct and incorrect trials. Triplets and quartets are combined as 'higher-order' coordination events. The dashed lines mark the significance threshold of the p-value (0.05). (B) Normalized coordination rates for pairs, triplets, and quartets, measured for the 300-ms window starting 150-ms after test onset (dots represent individual sessions). A hyperbolic scale was used for the y-axis to optimize representations for all sessions.

We further examined the correlation between the coordination rate and behavioral choice by performing an ideal observer analysis (Britten et al. 2009; Purushothaman and Bradley 2005; Nienborg and Cumming 2006) to predict the animal's choice on a trial by trial basis based on temporally coordinated events (Figure III-16A). For an example quartet, we represented the distributions of coordination rates for correct and incorrect trials and the corresponding ROC curves. The distributions of correct and incorrect trials were partially separated (the area under ROC was 0.66 which is comparable to the previously reported values (Britten et al. 2009; Purushothaman and Bradley 2005; Nienborg and Cumming 2006; Uka et al. 2005)). We illustrate the prediction of the ideal observer that uses the firing rates of the four neurons as well as coordination rates of the

6 possible pairs within the quartet. When using the firing rates, the average of the area under the ROC curve was 0.49 as expected by overlapping correct and incorrect distributions. When using coordination rates of pairs, the average area under the ROC curve was 0.55 as expected by greatly overlapping distributions of correct and incorrect coordination rates.

For our population of cell combinations (pairs, triplets, and quartets) we averaged the area under ROC curve for the test stimulus (150-500 ms time window relative to test onset) corresponding to each session. Figure III-16B represent the session-by-session changes in coordination rate (correct – incorrect) and the area under ROC for the test stimulus. The difference in coordination rates was only significant for triplets and quartets in V4 ($p < 0.0167$, Wilcoxon signed ranked test with multiple comparison correction. Combining across higher order combinations, p-value for monkey W was 0.001 and for monkey C was 0.039).

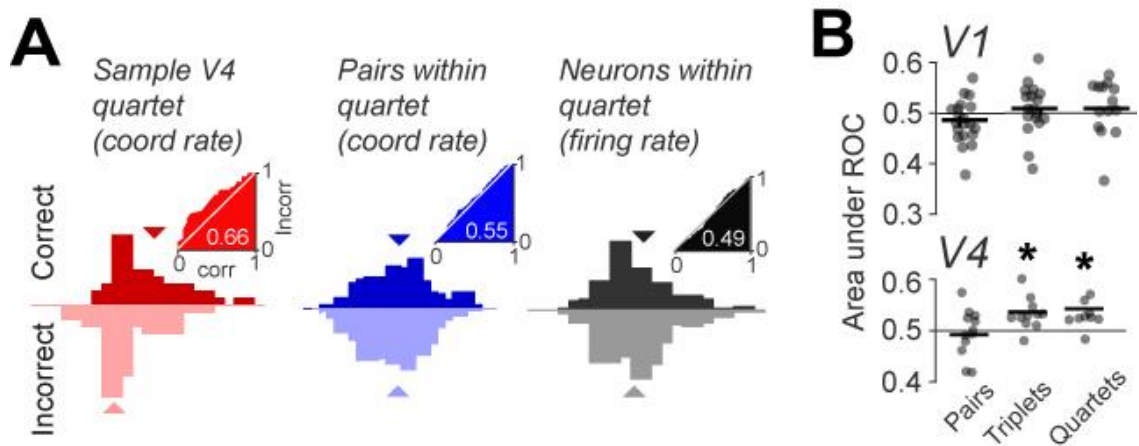


Figure III-16 (A) The distribution of coordination rates for (left) correct and incorrect trials for a sample quartet, (middle) all six possible pairs within the quartet, and (right) the firing rates of all four neurons within the quartet. Insets: ROC curves for correct vs. incorrect trials. (B) Area under ROC curve for correct vs. incorrect trials averaged across all coordination events of the same order (pairs, triplets, quartets) within each session (dots represent individual sessions).

Applying the same analysis to either target (150-500 ms after target stimulus onset) or delay (-350 to 0 ms before the test stimulus onset) period, we were unable to predict the behavioral choice using coordination rates of any assembly size ($p > 0.1$, Wilcoxon signed rank test). Also, for the test period, prediction of behavioral choice based on the coordination of triplets and quartets in V4 were consistent across sessions ($p < 0.05$, Wilcoxon signed ranked test) while the predictability of behavioral choice based on pairs of cells was not statistically significant ($p > 0.1$, Wilcoxon signed ranked test). In contrast, we were unable to reliably predict the behavioral outcomes based on the coordination of spikes within V1 (Wilcoxon signed rank, $p > 0.1$). Using the same window, shuffling trials yielded no significant difference between the two behavioral conditions.

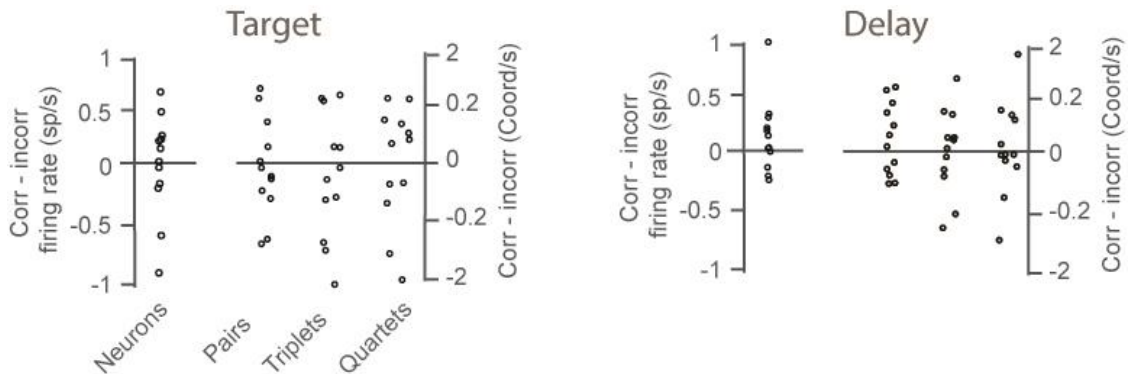


Figure III-17 Distribution of the difference in coordination rate between correct and incorrect trials for 12 V4 sessions during the target (left) and delay (right) intervals. The windows of analysis is identical to that in Fig. 3E. All analysis parameters are the same as in Fig. 3E.

We examined coordinated spiking at a range of time resolutions. While converging inputs within 1 ms can effectively drive postsynaptic targets (Zandvakili and Kohn 2015), coordination within the 10 ms range reflects multi-synaptic communication between participating neurons (Takeuchi et al. 2011a). Although our analysis was focused on coordinated spiking within 5 ms, we varied the time bin of the analysis from 1 to 11 ms.

We subsequently held the bin size to 5 ms and varied the jitter range from 3 to 13 ms. The differences in coordination rates increased monotonically with bin size and were significant for time bins of 4 ms or wider (Fig. S9A, top: coordination rate differences, bottom: p-value of Wilcoxon signed rank) and jitter range of 8 ms and higher (Fig. S9A, top: coordination rate differences, bottom: p-value of Wilcoxon signed rank). The ± 8 ms window allows for multiple synaptic transitions (Takeuchi et al. 2011b; Pipa et al. 2008). Therefore, the observed coordination in V4 can include multiple synapses between participating neurons which, by definition, is different from controversial effect of synchronized spikes discussed in (Shadlen and Movshon 1999; Histed and Maunsell 2013).

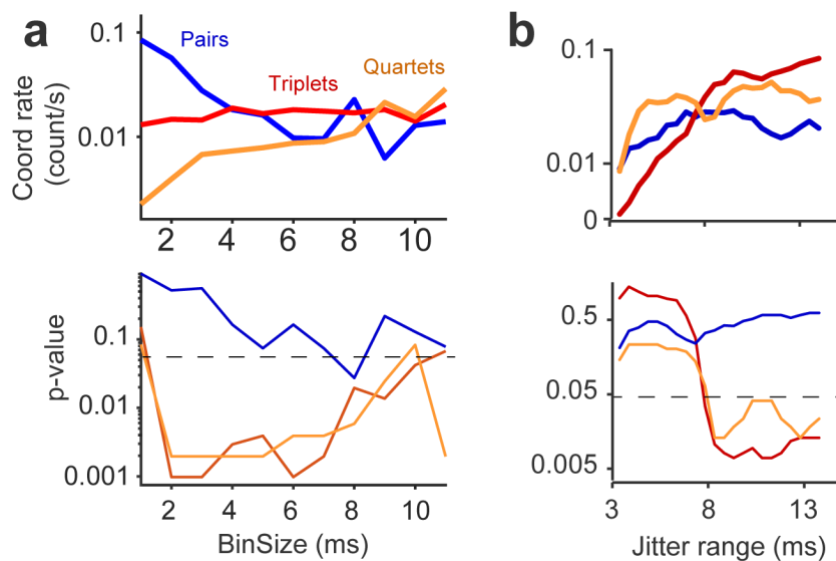


Figure III-18 Coordination rates were significantly different between correct and incorrect trials ($p < 0.05$, Wilcoxon signed rank test) for a range of bin sizes and jitter ranges. a) Coordination rates as a function of bin size (top) and associated p-values (bottom). The bin width varied in the range of 1 and 11 ms with steps of 1 ms. For bin sizes of 2-9 ms, p-values of triplets and quartets are smaller than 0.05. b) Same analysis as in (a) but for jitter range of 3 to 13 ms with steps of 1 ms. For jitter range of 8 ms and higher, the p-value was smaller than 0.05.

HIGHER ORDER EVENTS ACROSS V1 AND V4

Our results so far indicate that neuronal coordination within V4 higher-order ensembles carries information about the animal's behavioral choice. However, areas V1 and V4 are both directly and indirectly connected through feed-forward and feedback connections

(Felleman and Van Essen; Ungerleider et al. 2008). This raises the question of whether the coordination between V1 and V4 neurons is informative for behavioral decisions. We addressed this question by further examining the V1 and V4 neurons with overlapping receptive fields ($n=8$ sessions) and focused exclusively on the test stimulus interval where we previously found significant behaviorally relevant coordination in area V4. Specifically, we selected aligned spike trains in V1 and V4 within a 300 ms window, and then shifted the V4 spike trains relative to those in V1 by time τ (between -40 and 40 ms, in 5-ms increments). For each τ we pooled the spike trains and computed the coordination rates (Figure III-19, top), then we identified the peak coordination rate as well as the time lag at which this peak occurs. The statistical significance of the peak was determined by z-scoring coordination rates across τ values, similar to the cross-correlation analysis in (M. a Smith et al. 2012; Bair, Zohary, and Newsome 2001).

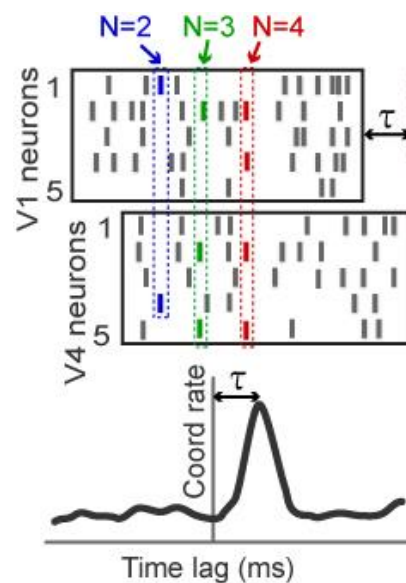


Figure III-19 Cartoon raster plots of V1 and V4 responses illustrating the magnitude and time lag of V1-V4 coordination. Coordination rates were calculated from spike trains from both areas by shifting the V4 spikes by time lag T (between ± 40 ms, in 5-ms steps). The peak coordination and time lag were determined after z-scoring coordination rates for all time lags by the average coordination rate of the tail (-40 to -20 ms time lag).

Furthermore, we identified the segment of the trial (test stimulus portion only) where the maximum coordination occurs. We did this by taking a 300 ms segment, starting 250 ms before the test stimulus onset and computing the cross correlation. These 300 ms segments were taken in 50 ms incremental steps. The final segment began 200 ms after the test stimulus onset. For 7 out of 8 sessions, a significant peak (z-score of 2 or higher) was found in correct trials for the analysis window that was centered at 100 ms after the test onset (**Error! Reference source not found.**).

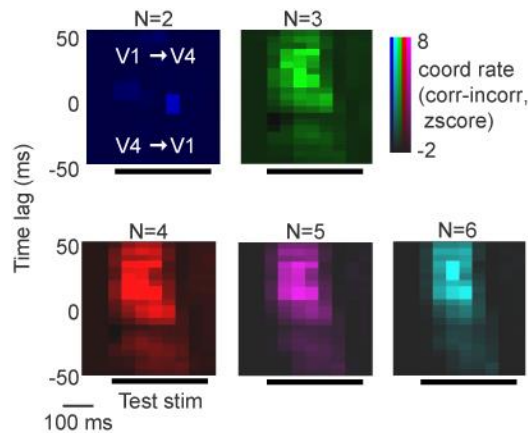


Figure III-20 Difference between coordination rates for correct and incorrect trials averaged across 8 sessions as a function of time lag. The peak coordination rate ($z\text{-score} > 2$) for higher order coordinated events occurs when V4 lags V1 by +25 ms, and around 100 ms after test onset.

For this analysis window, we found that in 7 out of 8 sessions the higher order coordination rates peak when V4 lags V1 by 20 to 40 ms (The peak of session average occurs around 25 ms, Figure III-21), consistent with previous reports of the delay of visual information between areas V1 and V4 (Leonard et al. 2011).

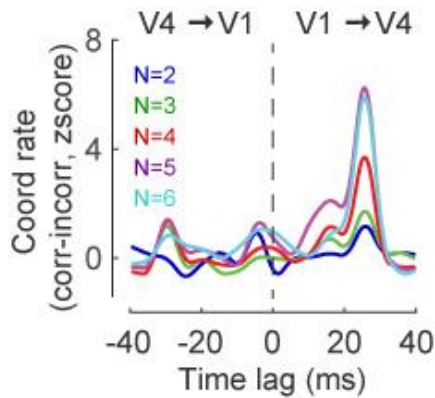


Figure III-21 Coordination rate (correct vs. incorrect) as a function of time lag for each event size was calculated for the 300-ms window overlapping the test stimulus presentation. The peaks for higher order coordinated events occur for feedforward communication (20-40 ms time lags; the average time lag across sessions is 25 ms).

Comparing the peak frequency of feedforward (V1 to V4) coordination across correct and incorrect conditions, we found that although the pairs of coordinated spikes were not different between correct and incorrect trials, the higher-order coordination (order 3 and above) depends on the behavioral choice ($p < 0.05$ Wilcoxon signed rank test, Figure III-22).

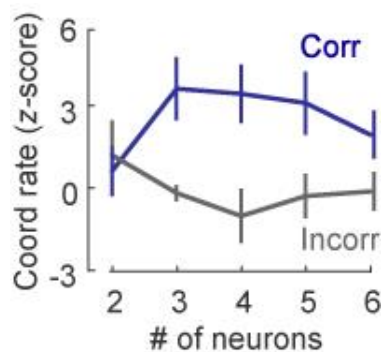


Figure III-22 z-scored coordination rates for correct and incorrect trials, calculated for the time lag corresponding to the peak in each session (we included 7 out of 8 sessions showing a significant difference between correct and incorrect trials; $p < 0.05$, Wilcoxon signed rank).

To investigate if the higher order events in V4 are triggered by higher order events in V1 or vice versa, we performed a cross correlation analysis between higher order events in V1 and V4. Again, we found a peak at 25 ms time lag in correct trials suggesting that

higher order events in V4 lag higher order events in V1 by 25 ms (Figure III-23). For incorrect trials we did not find any peak.

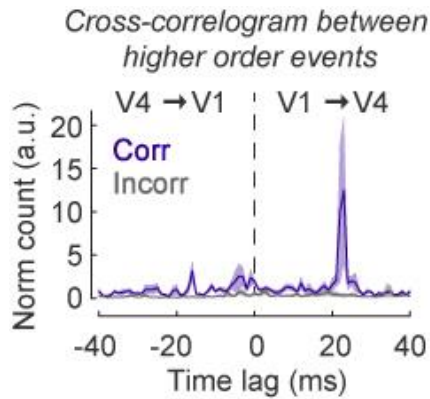


Figure III-23 Cross-correlation between the occurrence times of higher order events in V1 and V4 for correct and incorrect trials (5-ms bin size). The rates of co-occurrence of higher order events in V1 and V4 were normalized by the geometric mean of the occurrence rates. Error bars represent s.e.m.

Also, a pairwise cross-correlation analysis on spikes of individual neurons in V1 and V4 did not reveal any functional connectivity (Figure III-24).

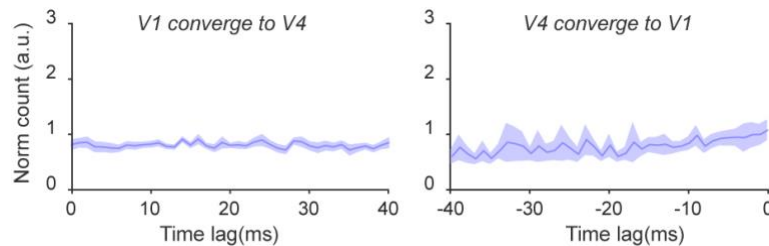


Figure III-24 We computed the cross-correlogram (CCG) between V1 and V4 to test whether high-order spiking coordination drives spiking activity in a target area. Left: CCG between convergent feedforward inputs from V1 (high-order spiking events) and V4 individual spikes reveals that high-order coordination in V1 is not associated with elevated spiking in V4. Right: CCG between convergent feedback inputs from V4 (high-order spiking events) and V1 individual spikes reveals that high-order coordination in V4 is not associated with elevated spiking in V1. Each cross-correlogram was normalized by the geometric mean of the firing rates of participating neurons. No significant CCG peak ($z\text{-score} > 2$) was observed within the ± 40 ms time lag range that we explored.

CONCLUSION

We calculated cross-correlation of simultaneously recorded pairs of neurons within area V1 and area V4 as well as between V1 and V4 to reveal the strength of the functional connectivity between neurons. Our hypothesis was that the strength of the functional connectivity would reflect the variation in accuracy of discrimination between two very similar stimuli. To examine this hypothesis, we calculated the magnitude of cross-correlogram peaks for the evoked response to each stimulus and compared the two. Moreover, we compared the magnitude of the peak of the correctly reported orientation change to that of the incorrect reports during the sustain response and after the response to a single stimulus. Although we found pairs of neurons in each cortical area for which the magnitude of peak was different between the two stimulus conditions or the two behavioral conditions, the overall change of magnitude was not systematic and not statistically significant. There are multiple reasons that the cross-correlation analyses failed to reveal any convincing effect:

- The cross-correlogram is a pair-wise method which is suitable to capture the diversity of functional connectivity across a population. The connectivity of pairs within a population may reflect local processing that are irrelevant to the perceptual goal. Given the high degree of connectivity of cortical neurons, dissecting the magnitude of the cross-correlogram peaks into local and global sources might not be possible.
- For cross-areas pairs, the chance that a task-irrelevant local source masks the perceptual effect is low. However, the main anatomical pathways between V1 and V4 pass through V2 and the direct connections, which potentially can be detected using cross-correlograms are only a small portion of both feedforward and feedback pathways.

- The high temporal resolution of cross-correlograms is offered at the cost of reducing the statistical power. To gain statistical power, previous studies have taken advantage of long recording time or high number of trials. Most of these studies were performed on anesthetized animals, for which the constrain on trial length and number is relaxed, or on awake animals that are simply fixating on simplified stimuli. Our experiment was limited in the number of trials and the duration of stimulus presentation which explain the noisiness of our cross-correlograms. The low statistical power means higher chance of both type I and type II statistical error. While in type II error, the chance of detecting the true functional connectivity is missed, in type I error, the false positive pairs that are mixed with the truly connected pairs mask the modulation of connectivity.

Taken together, cross-correlation is not a powerful method to reveal the modulation of connectivity in our experiment. In addition, because cross-correlation is pairwise, it does not capture higher order interaction within populations which, although rarer, might be more informative about a global effect such as perceptual processing. This was our motivation to explore population measures of connectivity. We used a powerful statistical method to identify coordinated spike event across the entire population. But first we show that even though this method is able to find coordinated events that the pair-wise methods cannot, it does not falsely identified co-occurrences of the spike events as coordinated events. Applying this method to V1 and V4 populations revealed modulation of coordination rate with behavioral performance within the V4 population but not V1 population. We also observed elevation of coordination rate between V1 and V4 considering a feed-forward time lag between areas. Both findings imply that the behavioral accuracy is due, at least in part, to facilitation of communication between

neurons that are encoding task-relevant information. The significance of this finding and alternative hypotheses will be further discussed in the following chapter.

Our findings reveal the existence of precise coordination of individual spike events in visual cortex time-locked to the onset of stimulus presentation. Although previous studies have shown that spike timing in the retina (Meister, Lagnado, and Baylor 1995; Gollisch and Meister 2008), thalamus (Dan, Atick, and Reid 1996), infero-temporal cortex (Hirabayashi and Miyashita 2005), and frontal cortex (Vaadia et al. 1995) carries information about specific stimulus attributes, we found that the precise coordination of high-order spiking events in visual cortex influences perceptual accuracy in the absence of firing rate modulation. However, while both early and mid-level cortical areas exhibited high-order spiking coordination, perceptual accuracy was associated only with high-order coordination in area V4. Surprisingly, despite common belief that extrastriate feedback projections carry information about behavioral decisions (Gilbert and Li 2013; Takeuchi et al. 2011b), we found that only feedforward coordination between spiking events is functionally relevant for perception. Thus, incorrect behavioral responses may be due, at least in part, to weak feedforward communication between sensory areas, which contributes to a loss of stimulus information along the feedforward pathway (Smolyanskaya et al. 2015).

We demonstrate that incorrect perceptual reports can be attributed to an improper decoding of sensory information in area V4, but not V1 (Figure IV-1). That is, although neuronal firing rates were not different between correct and incorrect trials in any of these two areas, only the neurons in V4 failed to encode the task-relevant stimuli when behavioral responses were incorrect. We further suggest that the reason for this failure of sensory information to reach V4 is the weak intracortical and cortico-cortical spiking coordination. Indeed, the signals from V1 must be accurately relayed to V4 and higher cortex to support accurate perception (Crick and Koch 1998; Felleman and Van Essen).

Consistent with previous theories (Fries 2005; König, Engel, and Singer 1996) we propose that the accurate transmission of neural signals from V1 may be accomplished by the precise temporal coordination between V1 and V4, and that within the V4 local circuits involved in stimulus processing. Further, the elevated spiking coordination in V4 could either increase the efficacy in driving downstream networks or contribute to an increase in cortico-cortical feedforward coordination to higher cortical areas to maintain an accurate stimulus representation required for a correct perceptual report. Thus, our findings support previous theories (König, Engel, and Singer 1996; Fries 2005) hypothesizing that neuronal groups communicate via the precise temporal coordination of action potentials.

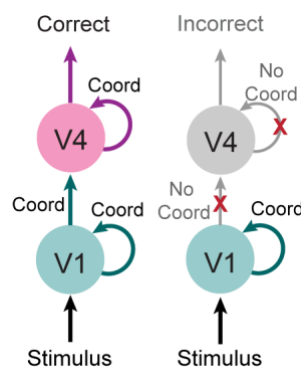


Figure IV-1 Cartoon depicting our conceptual model – V4 neurons decode the information from upstream areas (including V1). Spiking temporal coordination controls perceptual accuracy by modulating the efficacy of cortico-cortical signaling.

One apparently surprising finding is that feedforward, not feedback, V1-V4 coordination is related to perceptual accuracy. Indeed, since the extrastriate feedback to V1 is believed to carry top-down information about behavioral context (Lamme, Supér, and Spekreijse 1998; Ungerleider et al. 2008), we expected that correct behavioral responses would be correlated with feedback, not feedforward coordination. However, our analysis reveals that coordinated activity in V4 occurs after coordinated spiking events in V1, and that correct behavioral responses are associated with elevated V1-V4

coordination. From a functional standpoint, any neural mechanism relying on feedforward coordination of spikes is more efficient. Indeed, feedback coordination would require an extra 50-60 ms of processing time in order to transmit sensory information to higher cortical areas and influence perception. This suggests that inter-area spiking coordination may be optimized to facilitate stimulus transmission.

A possible limitation of our work is the lack of information regarding the identity of the neurons emitting spikes in each time bin. Indeed, in order to increase the reliability of our measurements, we calculated the coordinated activity in each trial without defining population “words”, and hence information about the spiking patterns among specific groups of visual cortical neurons that are most relevant for driving a correct perceptual report is missing. However, it has been suggested that complex network firing patterns can be accurately explained by considering the neurons’ firing rates and strength of population coupling (Okun et al. 2012), which is a measure related to spiking coordination. Furthermore, measuring population word distributions from array recordings in awake animals would be extremely challenging given our finite time trial structure and session length.

Our analysis indicates that V4 coordinated events are most likely due to V1 coordination propagated via feedforward pathways. However, an alternative scenario is that V1 and V4 coordination could instead reflect a common drive to these areas provided by an external source which enhances both V1 and V4 coordination. This is unlikely for the following reason. The cross-correlation analysis of coordinated events reveals a maximum at the expected temporal delay for signals from V1 to V4 (Ungerleider et al. 2008). Area V2, which receives the major output from V1 is likely to mediate, or contribute to V4 coordination, although it is unlikely to mediate coordinated spiking in V1 via feedback pathways. Indeed, if V2 neurons were the common source of coordinated

spiking in V1 and V4, we would have observed that, contrary to our findings, coordinated spiking events in V1 and V4 would occur almost simultaneously.

One potential concern in our study is cortical state. Indeed, it has been shown that during wakefulness visual cortex fluctuates through different states of synchrony (Beaman, Eagleman, and Dragoi 2017), and that the cortical state of local V4 populations is correlated with behavioral discrimination performance. Although cortical state may be likely to alter the strength of coordination, it would probably increase long timescale coordination rather than the brief timescale near-coincident spiking (within 5-ms bins) reported here. This is not an issue in our study, however, since the long timescale coordination was in fact removed as part of our controls when the jittered coordination rate was subtracted from the raw coordination. Furthermore, it was reported (Beaman, Eagleman, and Dragoi 2017) that increases in the low-frequency synchrony of local populations decrease perceptual accuracy, whereas we found interestingly that spiking coordination, our measure of brief timescale synchrony, increases it. Additionally, the Fano factor and noise correlations, which were previously correlated with attention (Mitchell, Sundberg, and Reynolds 2009; Reynolds and Chelazzi 2004; Cohen MR and Maunsell JHR 2009; McAdams and Maunsell 1999), were not significantly different between correct and incorrect trials in V4 (Figure IV-2; See Figure IV-3 as well for the statistics of the eye movements).

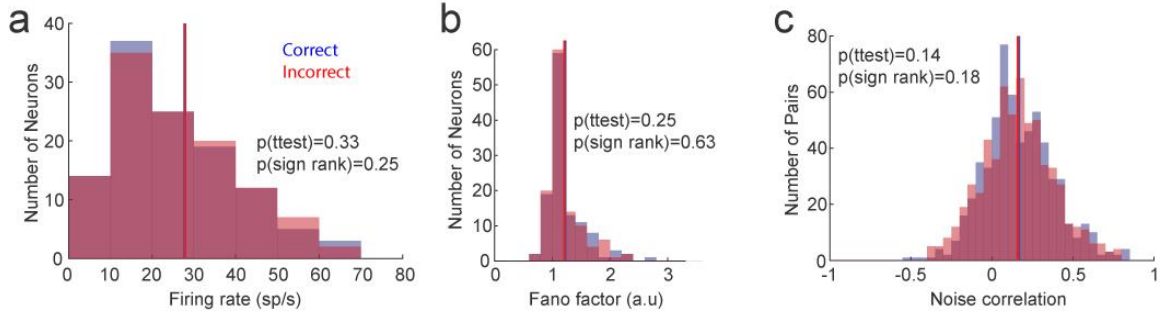


Figure IV-2 Three measures of neural activity in V4, previously demonstrated to be correlated with attentional modulation, do not exhibit significant differences between correct and incorrect trials. a) Firing rates of all V4 neurons across 12 sessions for the same time interval as in Fig. 3E. b) Fano factor of the firing rates of all V4 neurons. c) Noise correlations of simultaneously recorded pairs of V4 neurons

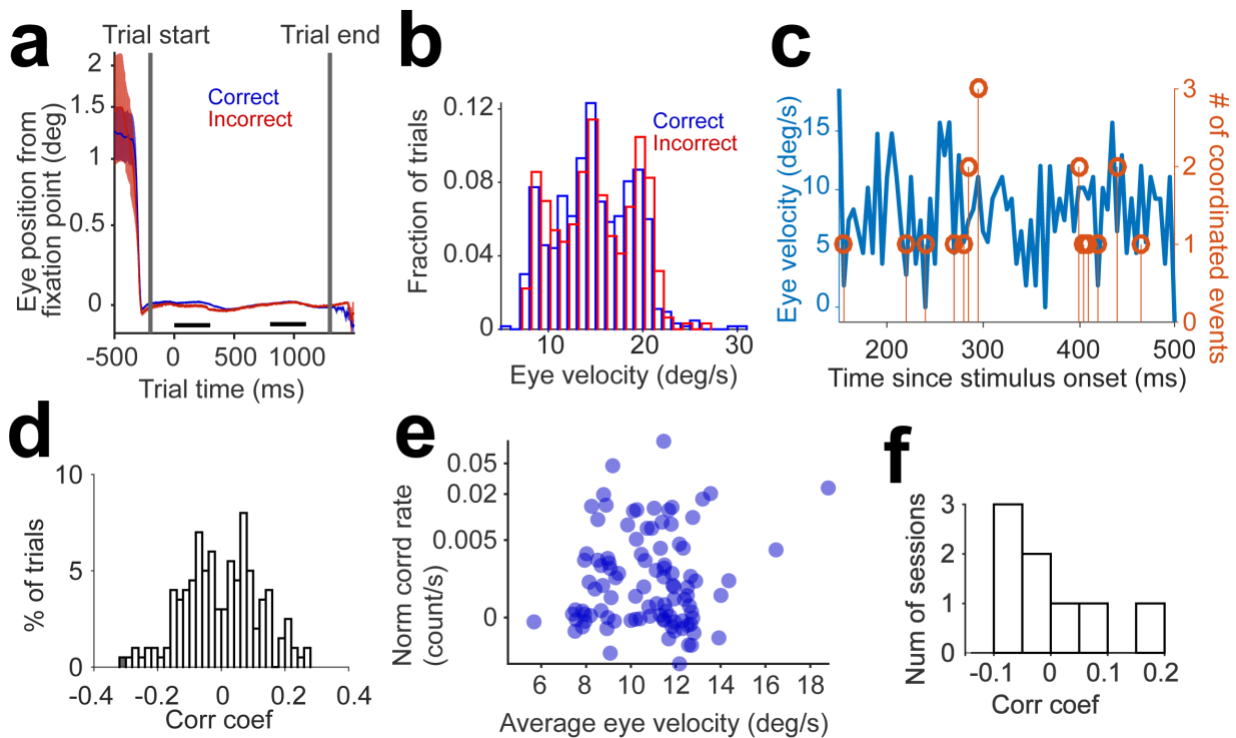


Figure IV-3 Coordination rates in V4 are unrelated to eye movements. a) The average traces of eye position as the distance from the fixation point, averaged across correct and incorrect trials on a sample session. b) Trial distributions of eye velocity for correct and incorrect trials are not statistically different for the same session in a. c) Single trial trace of the eye velocity (left y-axis) and number of coordinated events (right y-axis) for a sample trial. The length of time bins for both traces is 5 ms. d) The trial by trial correlation coefficient of two traces in c. for all trials of a sample session. The only trial with significant correlation coefficient ($p < 0.01$) is shown in black. e) The scatter plot of coordination rates and the eye velocity, calculated as the vector derivative of eye position, for all trials of a sample session. The correlation coefficient was 0.08 ($p > 0.4$). f) Distribution of correlation coefficients of eye velocity and coordination rates for all V4 sessions ($p > 0.2$ for all sessions).

Taken together, these findings provide supportive evidences for our hypothesis that in incorrect trials, stimulus information is lost in feedforward pathway probably due to weak communication. Future research will elucidate whether the encoding strategies revealed here – firing rate modulation to encode sensory inputs and precise coordination between higher-order assemblies to encode behavioral events – are restricted to early and mid-level visual cortex or whether they are components of a more general coding strategy found in other sensory cortical areas.

PART II

STRATEGY ENCODING IN PREFRONTAL CORTEX

*ABSTRACT_*Foraging animals explore the environment to earn valuable resources, at the lowest cost. Previous experiments on various species suggest that they simply maximize the current flow of rewards without predicting the future outcome of their actions. We found that monkeys are able to predict the reward outcomes to plan ahead, when allowed to forage freely in an interactive environment. In uncertain environments, the prediction of outcome requires access to a model of the reward structure. We recorded the activity of a population of individual neurons in dorso-lateral prefrontal cortex (dlPFC) and found representation of an internal reward model in this area. We singled out the component in dlPFC activity that represents the reward model and showed that this component predicts the next action. We think our naturalistic experimental setting as well as multi-dimensional analysis of the neural activity was the key to this finding and perhaps can shift the paradigm in studying neural correlates of complex behaviors.

CHAPTER V INTRODUCTION TO FORAGING AND OUR EXPERIMENTAL SETUP

Foraging is a natural task with direct implications in the life of modern humans. Foraging involves collecting valuable entities also known as reinforcements or rewards in uncertain environments. Existing theories of foraging strategy, which are based on decades of behavioral experiments on various species, revolve around melioration which is essentially maximizing the current flow of reward (Herrnstein, Rachlin, and Laibson 1997). However, the current flow of reward does not necessarily predict the future. Effective foraging requires building an internal representation of the structure of the environment to predict the value of each option and develop a strategy. Although there is no evidence of optimality of animals' foraging strategy, survival in environments with sparse resources requires that the animals are able to predict the outcomes before executing a costly action such as migration or relocation (Smith, 1982). The action planning and strategic decision making in the foraging task has not been well studied in laboratory settings. We think that one major challenge for studying animals' action planning in laboratory setting is the limitations of the classical paradigms. Essentially, in the laboratory designs of a foraging task, interactions of the animal with the environment is limited to choosing between predefined choices during a forced time window. This is despite the fact that, in many of the previous studies, the determining factor of reward scheduling was time (Sugrue, Corrado, and Newsome 2004; Schneider and Davison 2005; Herrnstein, Rachlin, and Laibson 1997; Gibbon et al. 1988; Aldiss and Davison 1979). Therefore, fixed structure of the foraging task and forced choice in the classical paradigms limit the ability of animals to exploit their full potential to understand the 'rules of the game'.

We designed a novel paradigm in which monkeys freely interact with an uncertain environment to understand the rules of the reward availability. Our paradigm has several advantages over classical experiments: First, Monkeys explore the environment with their own pace which allows them to execute a more deliberate strategy compared to their behavior in a forced choice task. Second, in our task, the reward sources are physically separated and exploring them requires relocation of the animal which is a natural way of enforcing a cost to their actions. Relocation, as the cost, does not require training the animals with complex associations (Shull and Pliskoff 1967; Sugrue, Corrado, and Newsome 2004). Finally, the freedom of movement allows the animal to be in a higher arousal state, compared to a restrained position, which improves their performance (Mcginley, David, and McCormick 2015).

One of the major challenges in studying the neural correlates of foraging in freely moving monkeys was recording the activity of individual neurons. The available tethering technology which has been used for rodents is obsolete with monkeys due to issues with safety of the animals and equipment. We solved this problem by using state of the art wireless electrophysiological systems that allow us to record neural activity in 96 channels with microsecond resolution (Yin et al. 2013, 2014).

We designed the behavioral task with two reward sources on independent variable-interval reward scheduling. The underlying mechanism of reward time generation was a simple Poisson process, but when the reward became available, it stayed available until collected. This process, although simple, has several interesting aspects: 1. The probability of reward availability is a function of time which mimics the natural characteristic of food availability in nature. 2. The probability of reward accumulates over time which implies that an unused resource usually has high chance of reward availability. This characteristic encourages exploration rather than exploiting the same

resource for a long time. 3. Although the average of inter-reward interval is determined, its range varies widely. Therefore, even when the distribution of inter-reward time is stationary, the prediction of reward availability is not trivial. For this study, we used stationary but independent distributions of inter-reward times for our two reward sources. When unbalanced distributions were used, we switched the distributions between two sides in the middle of the experiment as well as between experimental sessions.

We asked the question: “Can monkeys learn the characteristics of variable interval reward scheduling when allowed to freely explore reward options?” To understand the representation of the task in the brain, we recorded from population of individual neurons in dorso-lateral prefrontal cortex (dlPFC). Despite the fact that the value and reward are represented in many brain areas such as lateral and ventral prefrontal cortex (Kennerley and Wallis 2009), anterior-cingulate gyrus (Amemori, Amemori, and Graybiel 2015), infero-temporal cortex (Sugrue, Corrado, and Newsome 2004) and midbrain (Schultz n.d.), dlPFC is known for being involved in goal directed reward seeking behavior (Ridderinkhof et al. 2004; Rowe and Passingham 2001) which requires prediction of future reward outcomes based on an internal model of the reward availability. Areas in lateral PFC work together to integrate task-relevant information over time and use it to deliberately plan the next action (Fuster, Neuron, 2001). Given these evidences, we present our hypothesis and findings regarding the foraging strategy of animals in our free-moving foraging task and the involvement of dlPFC neuronal population.

The hypothesis

We expect to observe a more deliberate and complex behavior of monkeys in free-foraging task compared to previous reports of the same species in head-fixed setting as well as other species of animals such as rodents and pigeons. Perhaps, the deliberate

behavior we expect is mediated by areas in prefrontal cortex that represent the reward scheduling rules and elements of planned actions.

AIM 1. Understanding the behavioral strategy of the animals and predicting the next action.

AIM 2. Determining if the parameters of the foraging task are represented in the population of neurons in dIPFC, as an internal reward model.

AIM 3. Determining the components of neural activity that predict the next action.

The setup of the free-moving foraging task

The foraging environment was a custom made cubic cage (4'L x 2'W x 3'H) with two sources of reward on two sides of the longest dimension (Figure V-1). At each source of reward, the monkeys pressed a button or lever at any time. Once a button was pressed, the reward, if available, was delivered. A sound effect right after the time of the button push (less than 50ms later) cued the availability of reward. The reward is a 300 mg food pellet (Bio-serve or Test-diet) that is delivered using a pellet dispenser (med-associates). To record the neural activity wirelessly, 8 directional antennas were arranged strategically around the cage for the best coverage of the electromagnetic signal. To avoid electromagnetic interference, minimum amount of metal was used to build the cage and the apparatus. An overhead wide-angle camera was secured on the top of the cage for video recording.

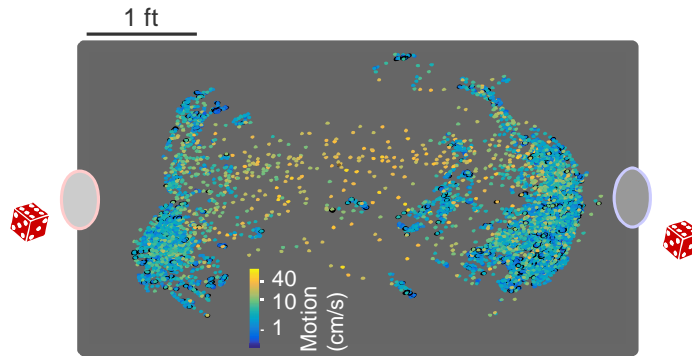


Figure V-1 The overhead view of the experimental cage overlaid with the location and motion (color coded) of the monkey every 200ms during an entire sample session. Two reward sources are at the ends of the longest dimension and are paired with push buttons or levers. The location and motion were calculated by image processing of the captured video (will be discussed in this chapter).

Variable interval reward scheduling

The availability of reward is determined using concurrent variable interval (VI) schedules. Briefly, the variable interval schedule relies on a Poisson process to determine the presence of reward. Once the reward emerges, it stays available until being collected by the monkey. Commonly, the variable interval schedule is called VI-M in which M is the expected inter-reward time in seconds. In concurrent scheduling, an independent Poisson process determines the availability of reward at each source and a switching cost between concurrent options was commonly used to balance the exploration and exploitation. When two sources are physically nearby, the switching cost is implemented by starting a time-out interval, also known as the change-over delay, every time that the monkey switches between the sources. In our task, switching between the sources of reward involved walking to the other side of the cage which takes much more effort than the effort required for pressing the lever at the same reward source. Therefore, we did not implement the change-over-delay, as the previous studies did.

Behavioral training and testing and human interventions

After habituating each monkey with the experimental cage, we trained them to press the button or lever and receive rewards. Over the course of 4-6 months we gradually

increased the mean time in the VI schedule to let the monkeys grasp the concept of probabilistic reward delivery. Once we started using VI10 (corresponding to an average reward rate of 0.1 rew/s) or higher (less than 0.1 rew/s), monkeys started to spontaneously switch back and forth between the two sources. If the monkeys disengaged from the task or showed signs of stress, we decreased the VI schedule (corresponding to increasing the reward rate) and kept it constant for one or two days. If the monkey showed strong bias toward one reward source, we used unbalanced schedules to encourage the monkeys to explore the less preferred source.

After training, we tested monkeys using a range of balanced or unbalanced reward schedules. For balanced schedules we used VI20 or VI30 on both sides. For unbalanced schedules we used VI20 vs VI40, VI15 vs. VI25 or VI10 vs VI30. The unbalanced schedules may reverse once, twice or three times during a session which means the side with VI20 will be VI40 and the side with VI40 will be VI20 after the reversal. Each session lasts until the monkey receives 100 or 200 rewards 1-7 hours including the 1-hour break after 100 rewards in sessions with 200 rewards. If the monkeys were not engaged with the task for more than 2 minutes, we sometimes interrupted to encourage them to engage with the task (For the analysis, we exclude all responses which occurred more than 100 s or less than 1 s after the previous response. The lower bound of the inter-response interval was enforced to avoid contamination in the event-locked neural activity).

Analysis of the location and the motions of the monkey

Each frame of the video from the over-head camera on the experimental cage was processed to determine the location and locomotion of the monkey (Figure V-2, step-1). First, the background image was calculated by averaging all frames in the same experimental session. To determine the location of the monkey in each frame, the

background image was subtracted from the frame (Figure V-2, step-2). The background removed image was then thresholded to find the dark areas (Figure V-2, step-3). The same image frame was also processed using standard edge detection algorithms (Figure V-2, step-4). The thresholded and edge detected images were then multiplied together and the result was convolved with a spatial filter, which was a circle with the rough diameter of the monkey in the over-head image (Figure V-2, step-5). The peak of the filtered image was found and marked as the location of the monkey (Figure V-2, step-6).

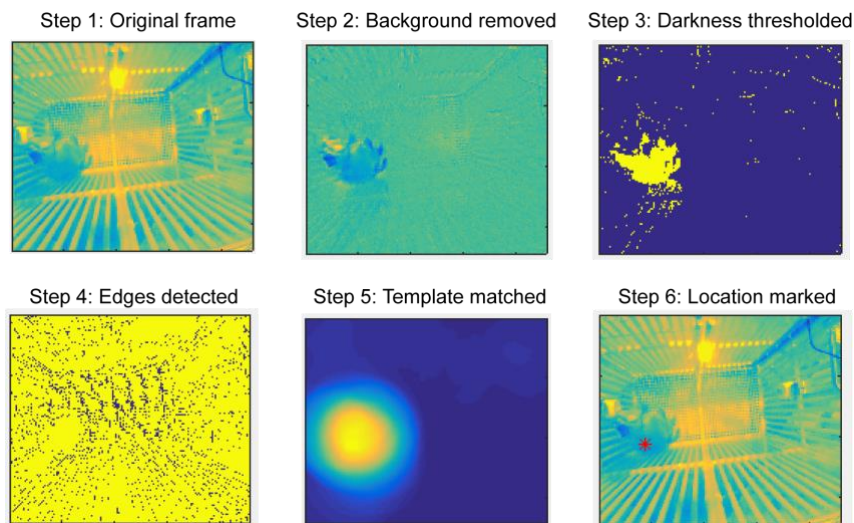


Figure V-2 Processing the images of the overhead camera to find the location of the monkey. See the text for description of steps 1-6.

Chronic implantation of the Utah array

We surgically implanted a 96-channel Utah array (Blackrock Microsystems) in dIPFC (anterior of the Arcuate sulcus and dorsal of the Principle sulcus (Figure V-3) of each monkey. The stereotaxic location of dIPFC was determined using MRI images prior to the surgical procedure. The array was implanted using the pneumatic inserter (BlackRock microsystems) after craniotomy and duratomy on the insertion site. The pedestal was secured on the skull (on the same side of the array or on the medial line) using either bone cement or bone screws and dental acrylic. Two reference wires were

passed through the craniotomy under and above the dura mater. After the implant, the electrical contacts on the pedestal were protected using a plastic cap for the duration of implant except the experiment time. The recording sessions started as early as 1 month and as late as 2 years from the surgery date.

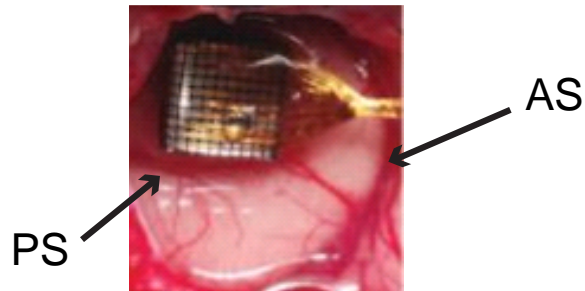


Figure V-3 The location of a 96-channel Utah array in dPFC on the left hemisphere of monkey G.

Recording and Pre-processing the neural activity

To record the activity of neurons while minimizing the interference with the behavioral task, we used a lightweight, battery powered device (Cereplex-W wireless system and Cerebus Neural signal processor, BlackRock Microsystems). First, the monkey was head-fixed, the cap was removed, the contacts were cleaned using alcohol and the wireless transmitter was screwed to the pedestal. The neural activity was recorded in the head fixed position for 10 minutes to ensure the quality of signal before releasing the monkey to the experimental cage.

The spikes were detected online using single or double thresholding of the raw electrical activity in each channel, then sorted to remove the artifacts that are introduced by the animal's movements, food chewing and general muscle activity. The perfect grounding on the circuitry of the chronic implant and the on-site amplification and digitalization of the signal in the wireless transmitter helped minimize the noise in our free-moving paradigm. The remaining noise was removed and the spikes from single neurons were sorted offline using the automatic algorithms in offline sorter (Plexon inc.). Briefly, this was done using the outlier removal in the space of the first three principle components

(outlier threshold = 4-5 x standard deviation), then the principle components were recalculated and used to sort single unit spike waveform using expectation maximization algorithm. A post cross-channel artifact removal procedure (custom code in Matlab) removes the waveforms that occur in more than 80% of the channels within a 1 ms time bin. Then each single and multi-units were evaluated using several criteria: showing consistent spike waveforms, modulation of activity during the 1 sec interval before or after the button pushes and exponentially decaying ISI histogram with no ISI shorter than the refractory period (1 ms). All spiking units with consistent waveform shape (single units) as well as the spiking units with mixed waveform shapes but clear pre or post modulation of firing rates (multi-units) were used (Figure V-4).

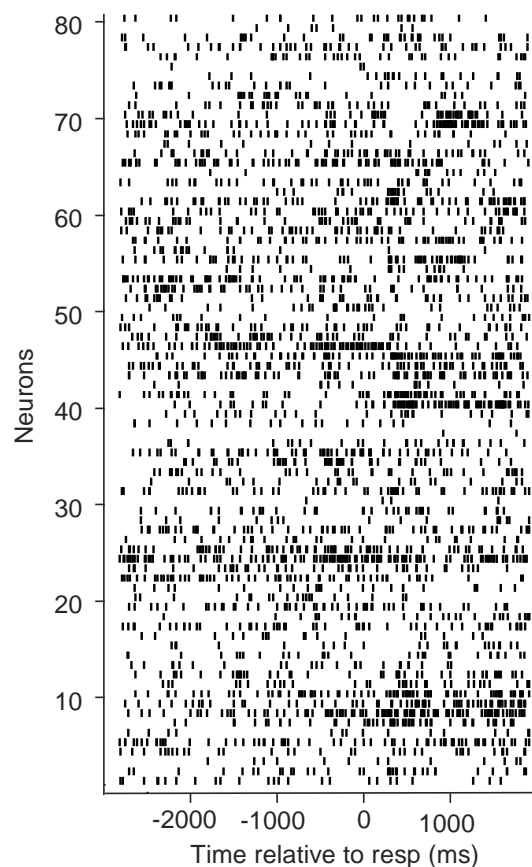


Figure V-4 Spike raster of 80 simultaneously recorded single and multi-units starting 3 s before and ending 2 s after a sample response.

CHAPTER VI ANALYSIS OF THE BEHAVIORAL STRATEGY

As discussed earlier, the central theory of foraging strategy in the previous studies revolves around the idea of melioration or matching law. Melioration is the process of maximizing the current flow of reward, without necessarily taking into account the prediction of future reward outcomes. In variable interval schedules, melioration results in assigning value to a reward source based on the current history of reward availability. In concurrent variable interval tasks, melioration results in choosing the option with the maximum local reward rate measured as the percentage of recent responses or trials that were rewarded. In variable interval reward scheduling, the local reward rate deviates widely from the mean reward rate. Therefore, in concurrent schedules, the reward ratios between options dynamically varies after each response. As a result, melioration strategy, which follows the local reward rate, leads to dynamically matching the time and effort to the option with maximum local reward rate. This observation is called ‘the matching law’ and it applies to observed behavior across various species. Usually, the matching is formulated as the equality of reward and response ratios. In the case of a two-choice task, the formula below conveys the matching law:

$$\frac{response_1}{response_1 + response_2} = \frac{reward_1}{reward_1 + reward_2}$$

At the first glance, matching law implies that the subject needs to estimate the reward schedules to be able to match response rate to reward rate. For example, if reward schedule is VI10 and VI20 for options 1 and 2, then, because the reward rate for option 1 is twice as option 2, the matching law predicts twice the number of responses on option 1 compared to option 2. However, we argue that the subject in the experiment does not need to know the ratio of the reward schedules to be able to match responses accordingly. In fact, a strategy that is blind to the ratios of schedules can result in

matching. This strategy, which we call the ‘win-stay-k-loss-switch’ or WSKLS, is as follows: The subject keeps choosing the same option unless not rewarded for k consecutive responses (k losses). If a response is rewarded, the number of losses resets to zero. When k losses occur, the subject switches to the other option and repeats the same algorithm until k losses occur again, in which case, he switches back to the first option. Basically, a subject following this strategy does not need to use any information regarding the scheduled rewards because the only parameter in this strategy is K which is blind to the schedules or their ratio. When we simulated this strategy, we observed that the response ratio matches, and precisely speaking, slightly under-matches, with the reward ratio. Interestingly, slight under-matching has been commonly observed across species, which implies that the subjects in the previous studies do not necessarily understand the actual reward rates or the rules of the variable interval reward scheduling.

Even though the number of losses (K_{loss}) is used by foraging animals to make decisions in VI reward scheduling, it is independent of the probability of reward availability (Pr_{rew}). The drawing in Figure VI-1 demonstrates an example case: The reward availability is determined in every time bin (10 ms) by a probabilistic process (Figure VI-1, top row). The probability of reward availability is calculated as

$$Pr_{\text{rew}} = 1 - (1 - p)^T$$

In which p is the probability of reward availability in every time bin and T is the number of time bins since the last response. This formula implies that the probability of reward availability increases exponentially with time and converges to 1, and after each response it resets back to 0 (second row). 6 sample responses are shown from which the 1st, 2nd, 3rd and 6th are rewarded (3rd row) because they occur when the reward was available. Although Pr_{rew} is the highest for the 6th response because it occurs after a long

wait after the 5th response, the K_{loss} for this response is 2 which is the biggest (last row). On the other hand, K_{loss} was 0 for the 2nd, 3rd and 4th responses, where the Pr_{rew} for these responses is not the highest.

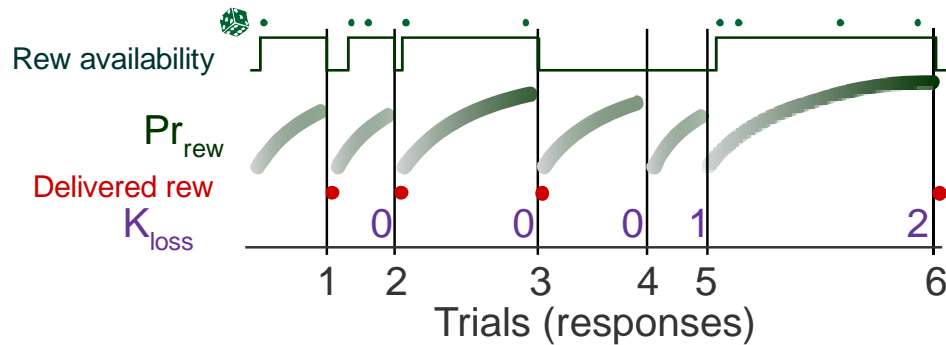


Figure VI-1 A Cartoon of variable interval reward schedules for 6 hypothetical trials which are the animals' responses. Rows from top to bottom: The Poisson process determines the reward probability in each time bin, the reward availability which takes a binary value, the probability of reward availability calculated as explained in the text, delivered reward as a binary variable and the number of losses which is the number of responses since the last reward.

Analyzing 89 experimental sessions from two monkeys also showed that the reward outcome is independent of the reward history but not the theoretical probability of reward availability. We calculated the percentage of rewarded trials for K_{loss} between 0 and 15 (which accounts for 71% of 30,958 trials) and Pr_{rew} between 0 and 1 (Figure VI-2), and we found that it is independent of K_{loss} while changing linearly with Pr_{rew} , as expected.

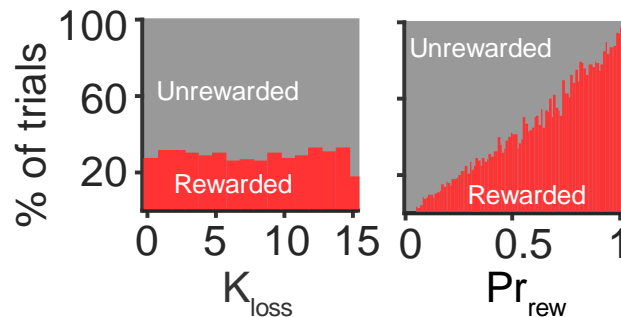


Figure VI-2 The histogram of the percentage of rewarded trials (responses) as the function of K_{loss} (left) and Pr_{rew} (right). 30,958 trials from 89 sessions of two monkeys were combined.

The analysis of matching behavior for the free-moving foraging task

We tested matching on the behavioral outcomes of all experimental sessions with reward schedules in the range of VI10 to VI40 by calculating the reward and response ratios. We also simulated WSKLS strategy in which the reward schedules on two sides varied between VI10 and VI40 independently. The distribution of inter-response times in the simulation was set as an exponential distribution with the mean of inter-response time for monkeys (4 s). We set k to be sampled from a normal distribution with mean of 3 which is the mean of the K_{loss} for the trials in which the monkeys switch to the alternative option afterward. We observe near matching behavior in both monkeys as well as the simulated WSKLS strategy (Figure VI-3). We also simulated two extremes strategies in which the subject persists on either side, meaning that K for that side was 10 times larger than the other side (We used $K=10$ for side 1 and $K=1$ for side 2 to simulate the strategy of persisting on side 1 and vice versa). These strategies resemble the case where the subject is strongly biased toward one of the sides. Comparing the performance of the monkeys to three simulations (WSKLS, persist on 1, and persist on 2) shows that their performance is closest to WSKLS strategy, which implies that the monkeys are following the history of rewards on both sides rather than having a strong bias toward either side (Figure VI-3).

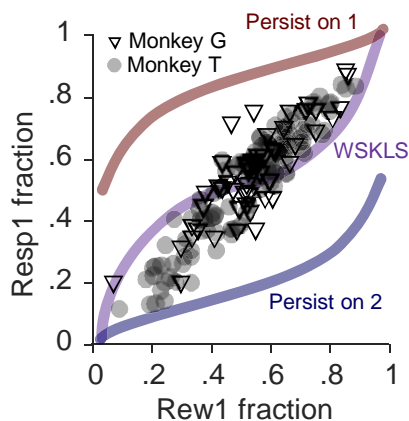


Figure VI-3 The matching behavior of monkey G and monkey T measured as the fraction of responses on side 1 as a function of the fraction of rewards on side 1. Also, the outcome of simulation of three strategies: WSKLS, persistence on side 1 and persistence on side 2, as explained in the text.

We further investigated the inclination of monkeys toward the side with the rich schedule or the side with poor schedule. We averaged K_{loss} before each switch on the rich side and on the poor side in each session and observed unbiased distribution of number of losses (Figure VI-4).

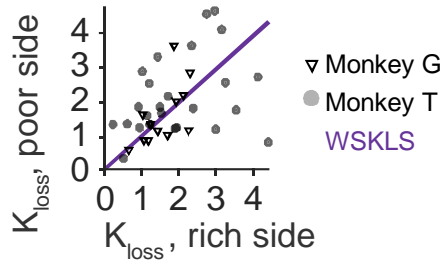


Figure VI-4 The scatter of the number of losses before a switch occurs on the rich and poor sides when imbalanced reward schedules were used, averaged within each session. The unity line represents the WSKLS strategy, a shifted scatter to below the unity line represents insisting on the rich side and a shifted scatter to above the unity line represents insisting on the poor side.

We also examined the dynamic matching by calculating the reward and response ratios locally. Within a window of 30 trials that slides across trials of each session, we calculated the reward and response ratios. We used a causal window, meaning the ratios were always calculated in the past 30 trials. We also used an exponential temporal filter as in (Sugrue, Corrado, and Newsome 2004) so that the most recent trial has the largest weight compared to the other trials within the window. Finally, we calculated the average reward and response ratio for the trials in the same session for which the schedules were constant. Figure VI-5-top shows an example session in which the schedules reverse twice after the monkey collects 35 and 135 rewards (this number is implicit in the figure because on the x-axis we show the number of trials rather than rewards). Compared to a simulated WSKLS strategy with the same parameters as the experimental session (Figure VI-5-bottom), the quality of matching is very similar (both session shows slightly lower response ratios compared to the reward ratios).

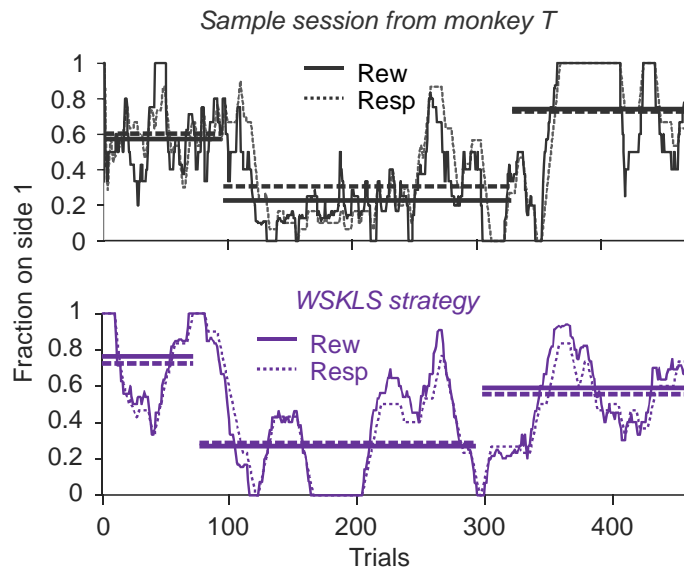


Figure VI-5 Dynamic of the reward and response ratios calculated for a window of 30 trials prior to the current trial for a sample experimental session (top) and simulated WSKLS strategy (bottom).

Taken together, the strategies that the monkeys follow cannot be separated from a blind WSKLS strategy when the behavior was analyzed using the matching law. In fact, the matching law explains the observed behavior without specifying the exact behavioral strategy. In the following section, we use a different approach to determine the behavioral strategy by predicting the next action using the parameters of the reward model as well as the actual reward outcomes.

Determining the foraging strategy and predicting the next action

As we previously discussed, the history of reward in variable interval reward scheduling is independent of the probability of reward availability. This implies that if the animal is simply meliorating, he is choosing his action solely based on the reward history and not the prediction of the future reward. To determine if the prediction of the reward outcome plays any role in the animals' decision making, we calculated Pr_{rew} for each response

and asked if the animals' next action can be predicted based on the history of reward (K_{loss}), the probability of reward availability (Pr_{rew}) or both. We define the next action using two parameters: 1. Choice, which is *staying* on the same reward option for the next response or *switching* to the other option and 2. Time until next response (TUNR), which determines how long the monkey waits before responding again, only when his choice was to *stay* on the same side.

To determine the effect of K_{loss} and Pr_{rew} on the choice, we separated all unrewarded¹ trials with 0, 1, and 2 losses, sort each group based on the Pr_{rew} , and calculated the percentage of *switches* within a 1000-trial sliding window (Figure VI-6). We observed that the percentage of *switches* increase with both K_{loss} and Pr_{rew} .

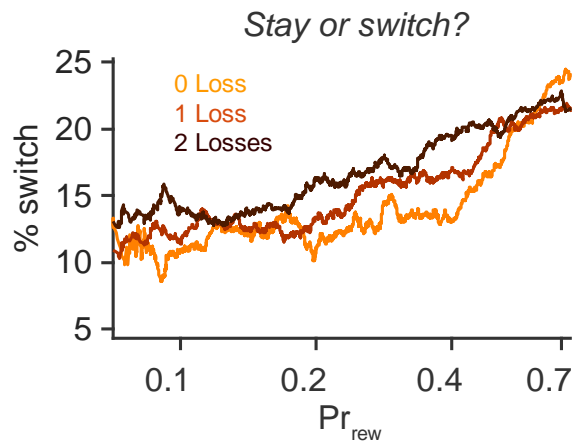


Figure VI-6 The percentage of switches for the trials for which the number of losses was 0, 1 and 2 as a function of the Pr_{rew} . The percentage of switches was calculated within a 1000-trial sliding window.

Similarly, we determined the effect of the probability of reward on the TUNR as follows:

We combined all trials for which the choice is to *stay* on the same side and the K_{loss} is in the range of 2 and 5 (basically not including the extremes on the K_{loss}). We also

¹ We excluded all rewarded trials from the choice analysis because both monkeys chose to *stay* in 99% of the rewarded trials.

separated the trials based on the reward outcome (rewarded vs. unrewarded). Then, we separated the 10% of trials with the lowest and 10% of trials with the highest Pr_{rew} in both groups of rewarded and unrewarded trials. This leads to four categories: low Pr_{rew} , unrewarded, low Pr_{rew} , rewarded, high Pr_{rew} unrewarded and high Pr_{rew} , rewarded. We sorted the trials in each category based on TUNR and compared the sorted histograms (Figure VI-7). We observed that the shortest TUNR occurred when Pr_{rew} was low, but the reward was delivered (the surprise reward) and the longest TUNR occurred when Pr_{rew} was high, but the reward was not delivered (the surprise miss). The TUNR for the two other categories were in between.

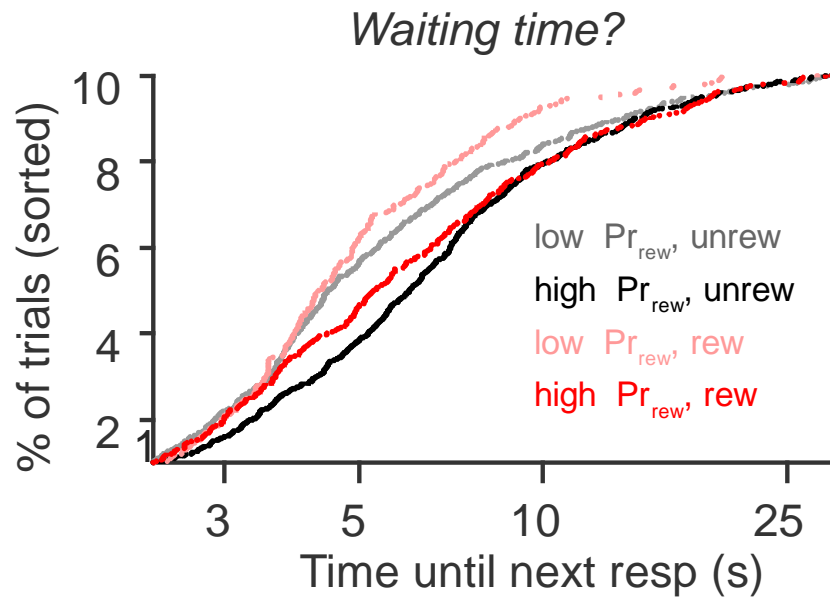


Figure VI-7 The histograms of TUNR for four categories of trials. The low/high Pr_{rew} trials are each 10% of the total trials (30,958 trials combined across 89 sessions) that are lower/higher than the 10/90 percentile. Trials in each category were sorted ascendingly using TUNR values.

Our findings imply that the monkeys 'expectation of reward' might be an estimation of the actual Pr_{rew} in this experiment and they would adjust their next action based on their expectation of reward as well as the actual reward (Figure VI-8).

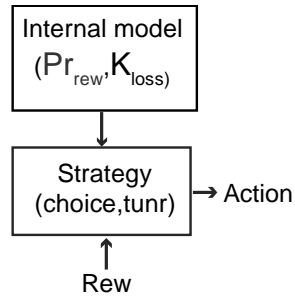


Figure VI-8 A cartoon of the suggested foraging strategy for predicting the next action in a trial by trial basis. The inputs of the strategy come from the internal reward model, which determines the reward expectation of the animal, as well as the actual reward outcome of the current trial. The next action (stay/switch and if stay, the time until the next response) will be planned using rules of the animal's foraging strategy.

Summary of results and discussion

To summarize our findings with the animals' strategy as a function of K_{loss} and Pr_{rew} , we trained regression models for choice and TUNR. To predict the choice, we trained a linear regression model on unrewarded trials using \log of K_{loss} and \log of Pr_{rew} as the input and the binary choice as the output. To convert the output of the regression models to a binary prediction of choice, we thresholded the output so that the total percentage of predicted choices was equal to the total percentage of actual choices. Similarly, we trained regression models with TUNR as the output for rewarded and unrewarded trials separately. Figure VI-9A summarizes the following strategy: Generally, when the monkeys were rewarded, they responded faster next time and were not likely to switch. If unrewarded when Pr_{rew} was high, they increased the TUNR. However, they were more likely to switch to the other side, instead of increasing TUNR, if K_{loss} was high, similar to WSKLS strategy. To determine the statistical significance of the model prediction, we cross-validated the regression models by dividing the trials to 20 sub-groups and testing the prediction performance on each subgroup while all other 19 groups were used for training the model (this procedure was repeated 100 times). The performance of the predictor of the choice, which was a binary variable, was calculated as the percentage of correctly predicted switches, while the performance of the predictor of TUNR, which was

a continuous variable, was calculated as the correlation between predicted TUNR and actual TUNR. The null hypothesis was the predicted performance of the models which were trained using shuffled data. We also trained models using either of the reward model parameters to compare to the predictors that were trained using both parameters. Figure VI-9B shows that the models using both Pr_{rew} and K_{loss} or only Pr_{rew} performed better than chance, but the models using only K_{loss} did not ($p < 1e-4$ when both parameters were used, $p < 0.03$ when only Pr_{rew} was used, and $p > 0.5$ when only K_{loss} was used, Wilcoxon signed rank test with FDR multiple comparison correction).

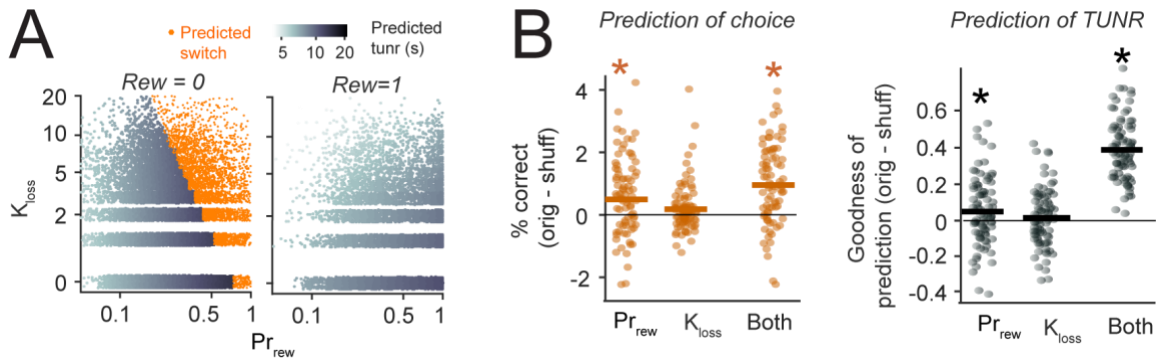


Figure VI-9 Prediction of the monkeys' next action. A) the graphical representation of the regression models that predict the next action using the parameters of the internal model as well as the reward outcome. B) Prediction performance of the models in A when the predictors use Pr_{rew} , K_{loss} or both

Taken together, our findings suggest that the history of reward (K_{loss}) as well the probability of the reward availability (Pr_{rew}) predict the next action of free-moving monkeys in the foraging task. We suggest that these two parameters represent a model of the reward scheduling in the monkeys' brain. In the next chapter we will provide evidences that both of these parameters were represented in the activity of neurons in dIPFC.

In this chapter, we investigate representation of the internal reward model in the activity of neurons in dlPFC. We expect that the activity of neurons in dlPFC represent a variety of task relevant and task-irrelevant factors. We are interested to determine the neural correlates of the task relevant parameters while avoiding contamination of our findings with neural correlates of the task irrelevant parameters. For example, the location of the monkey in the cage as well as the locomotion are task irrelevant parameters that are potentially modulating the neural activity (Figure VII-1).

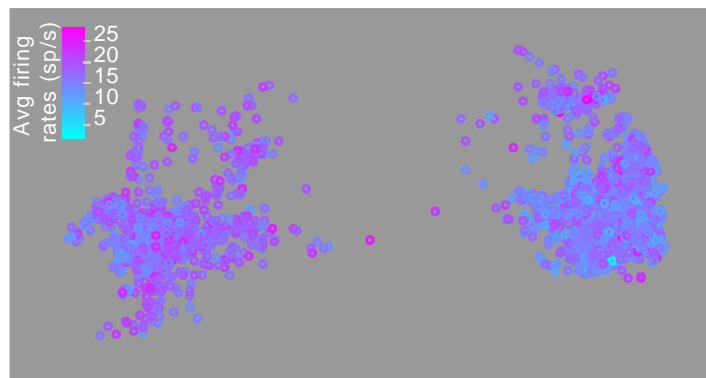


Figure VII-1 Population averaged firing rate for the pre-response period (-1.2 to -0.2 s) as a function of location of the monkey in a sample session. The location where determined using the image processing technique that we presented in CHAPTER V. Both the population averaged firing rate and the location vector were binned using 200 ms time bins.

Therefore, before we analyzed the correlation of the neural activity and the parameters of the internal model, we decorrelated them from the location and locomotion as presented in the next section.

Decorrelating the neural activity from the task-irrelevant parameters

To decorrelate the neural activity from the task irrelevant parameters, we used Gram–Schmidt orthogonalization process (Strang 2016). First, we designed a three-

dimensional space with task irrelevant parameters which are the monkey location in two dimensions (locX and locY) and the locomotion which was the vector difference of the location (locD). Then we removed the projection of the firing rates of each neuron on each orthogonal basis vector on this three-dimensional space. Figure VIII-2 shows the correlation matrix of neurons and the task irrelevant parameters before and after the orthogonalization.

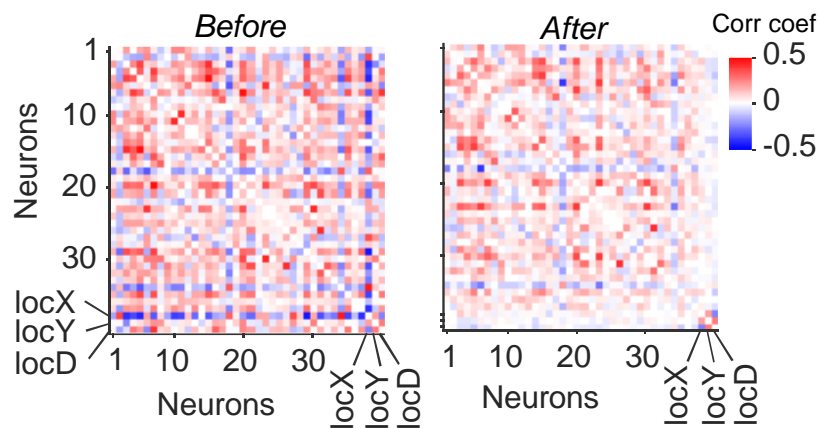


Figure VII-2 Correlation matrix for all neurons in the same session as well as the task-irrelevant parameters before(left) and after (right) the orthogonalization procedure.

The orthogonalization intends to remove the correlation between the neural activity and the task-irrelevant parameters, but not necessarily the correlation within the neuronal population or within the parameters themselves.

Decoding Pr_{rew} from the population activity

To determine the correlation of the pre-response firing rates with the Pr_{rew} , we first compared trial averaged peri-response time histograms of firing rates for high and low Pr_{rew} subsets, determined as the highest and lowest 20 percentile of the distribution of Pr_{rew} over the trials of each session (Figure VII-3).

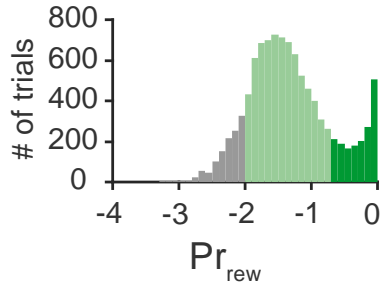


Figure VII-3 The distribution of the log probability of the reward availability for all responses combined across 22 sessions of two monkeys. The responses for which the inter-response time is smaller than 1s or bigger than 100s are removed.

Figure VII-4 shows a sample neuron for which the pre-response firing rate is higher for trials with high Pr_{rew} compared to the trials with low Pr_{rew} . To quantify this effect, we averaged the firing rates for the pre-response time interval (defined as 1.2 s to 0.2 s before the response time in each trial), then calculated the Pearson correlation coefficient between firing rates and logarithm of the reward probability (Figure VII-4, inset).

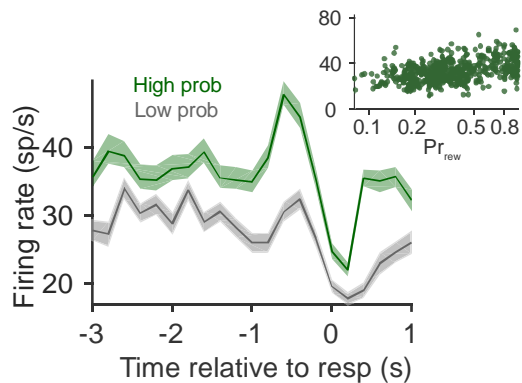


Figure VII-4 the firing rate of the same neuron for each 200ms time bin starting -3s and ending 1s relative to the time of the response averaged for 20th and lower as well as 80th and higher percentile of responses for the log reward probability. Inset: A sample neuron showing a positive correlation between the pre-response (-1.2 to -0.2 s) firing rate and the probability of reward availability for each response.

We found that for about 36% of individual neurons in two monkeys (28.6% of neurons in monkey G and 38% of neurons in monkey T), the pre-response firing rate significantly modulates with the probability of reward availability. The average of the distribution of correlation coefficient across neurons was 0.07 which was significantly bigger than zero

($p < 3e-38$ Wilcoxon signed rank test) meaning that more spikes are generated when the probability of reward availability is higher. This finding is consistent with previous studies suggesting that the extra spikes generated before a valuable motor action increases the precision of execution of that action (Ramkumar et al. 2016).

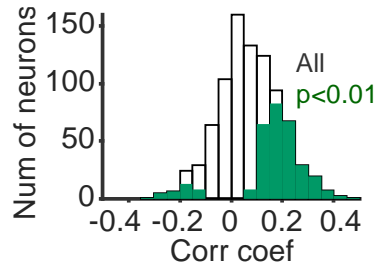


Figure VII-5 Distribution of correlation coefficients between pre-response firing rate and Pr_{rew} for all neurons combined across 22 sessions of two monkeys. The green sub-population has significant correlation coefficient ($p < 0.01$)

We were also able to decode the probability of reward availability from the neural activity on a trial by trial basis. We trained a linear regression model using the neural activity of the entire simultaneously recorded population, then used it to predict Pr_{rew} . To determine if the prediction performance is better than chance, we cross-validated the prediction and compared to the prediction of another regression model that was trained using shuffled trials. Figure VII-6 shows the predicted Pr_{rew} vs. the actual Pr_{rew} for the original and shuffled regression models. To quantify goodness of fit, we calculated the correlation coefficient of the predicted Pr_{rew} and the actual Pr_{rew} for the original and shuffled models. Therefore, the goodness of fit is always in the range of ± 1 . Figure VII-6, inset shows the goodness of fit for all sessions. The Pr_{rew} was predictable in 21 out of 22 sessions ($p < 6e-23$, Wilcoxon signed rank test).

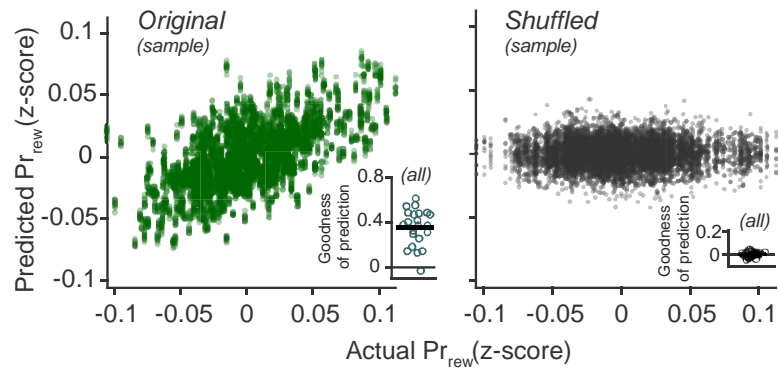


Figure VII-6 Actual vs predicted probabilities of reward availability. Insets: The goodness of prediction (correlation between actual and predicted) for all sessions

We also examined the effect of the size of the neural population on the prediction performance by using a random subset of neurons as the input of the regression model. We repeated the analysis for sub-populations of size 1, 5, 10 up to the number of recorded neurons in each session with 20 random subsets for each sub-population size. We observed that the performance always improves when more neurons are participating, but the rate of improvement saturates when the population size is bigger than around 15 neurons (Figure VII-7).

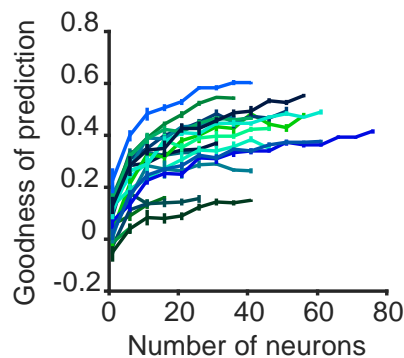


Figure VII-7 prediction performance as a function of the number of neurons used. Each line represents a session. A total of 22 sessions were tested.

Decoding the K_{loss} from the population activity

We performed a similar analysis to show that the K_{loss} is encoded in the neural population as well. The activity of two example neurons are shown in Figure VII-8A.

While the neuron on the left panel generates more spikes when K_{loss} was in the higher 20th percentile compared to the lower 20th percentile, the neuron on the right panel shows the opposite. The modulation of pre-response activity of these two neurons to K_{loss} was also quantified by calculating the correlation coefficient between the log of k_{loss} and the firing rates within the pre-response interval (Figure VII-8A, insets). The distribution of correlation coefficient across all recorded neurons showed that the percentage of neurons sensitive to K_{loss} was lower than the percentage of neurons that were sensitive to Pr_{rew} (Figure VII-8B). A decoding analysis, with the exact same setting of the decoders that were trained for Pr_{rew} , confirm modulation of population activity with K_{loss} (Figure VII-8C and D).

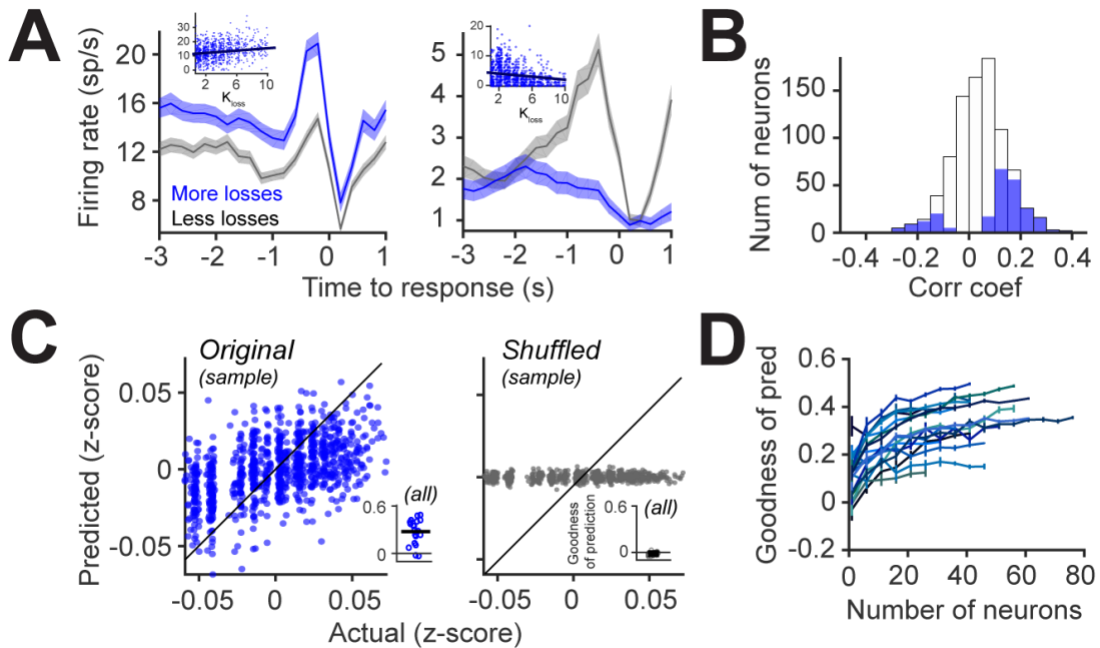


Figure VII-8 The history of reward (K_{loss}) was encoded in the population activity. The details of the analysis were exactly the same as what we explained for Pr_{rew} .

Summary of results and Discussion

We found that parameters of the internal reward model are represented in pre-response activity of individual neurons in dlPFC. Although a considerable percentage of individual single or multi-units show significant correlation with the task parameters, the performance of decoders of the internal model parameters is not consistently above the chance for individual neurons but improves when more neurons are used for decoding.

Our finding that K_{loss} is represented in the neural activity was not surprising, since previous studies show that individual neurons in infero-temporal cortical areas or prefrontal areas represent the local history of reward. However, to our knowledge, none of the previous studies show a modulation of neural activity with the actual probability of reward availability in any brain areas. This finding is significant because this parameter is not observable to the monkeys. However, as we showed before, the probability of reward availability in variable reward scheduling is a function of the time interval between the responses. We think the lack of previous reports on encoding this parameter might be due to the fact that none of the previous studies on variable-interval reward scheduling allow the animal to interact with the task in flexible time intervals.

The fact that we found the representation of the reward model in pre-response neural activity suggests that the neurons represent the expectation of reward. Together, with the results that were reported in the previous chapter, our findings suggest that the monkeys build an internal representation of the reward schedules and use this model to estimate the expectation of reward and, consequently, use the internal model to decide on their next action. In the next chapter, we discuss how the neural activity predicts their strategy.

In the previous chapter, we provided evidences that both parameters of the internal reward model, the history of reward (K_{loss}), and the probability of reward availability (Pr_{rew}), are represented in the pre-response activity of neurons and they can be decoded from the activity of a decent size population. In this chapter, we ask the question: Are these two reward model parameters represented separately in sub-populations of dIPFC neurons or do their representations have a common source? In another words, the reward model parameters might not be the actual parameters that are encoded in the population of neurons separately, but only correlated with other task-relevant components that are actually encoded in the population of neurons. We used Canonical Correlation Analysis (CCA) (Thorndike 2000) to identify these components (Figure VIII-1). If each component is composed of only one of the reward model parameters, then we can conclude that the reward model parameters are encoded in the population separately. However, if the components are a mixture of both reward model parameters, then we conclude that some other actual task-relevant parameters, which may or may not have an explicit interpretation, are encoded in the neural population. To avoid a situation that the components are composed of many small portions of parameters or neurons, we enforce sparseness criteria. The concept of sparse CCA is explained in the following section.

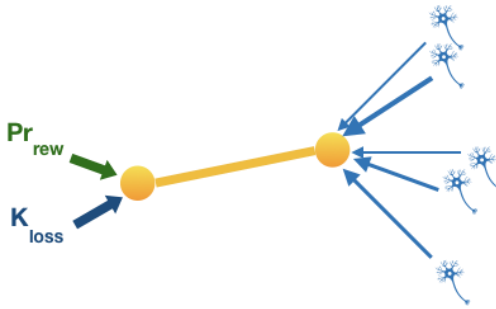


Figure VIII-1 We used Canonical Correlation Analysis to find pairs of components (yellow), one in the space of the reward model parameters and one in the space of the simultaneously recorded individual neurons. The main characteristic of the component pair is that they are correlated stronger than any other combinations of parameters with any other combinations of neuronal activity.

Sparse canonical correlation analysis

Although correlation analysis is immensely popular in understanding neural codes, a correlation between two entities do not specify whether they are directly related or confounded by a shared source. CCA has been used to identify shared sources that might not be directly observable but generate correlation among various entities. Essentially, CCA is one step forward to separate direct correlations from induced correlations which are correlations that are mediated by shared sources (Figure VIII-2). Technically, to find canonical components on two sets of random variable X and Y , we first calculate the co-variance matrix of $X'Y$, then apply singular value decomposition on the covariance matrix. The number of components is equal to the rank of the covariance matrix which is always equal to, or smaller than, the minimum of the number of variables in X and Y .

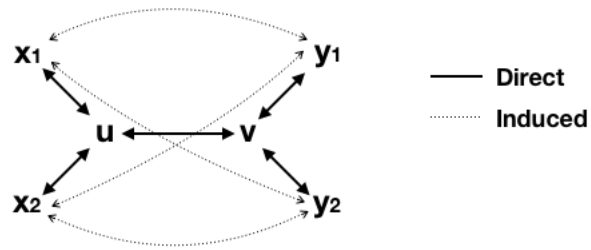


Figure VIII-2 Correlation between random variables can be direct (solid) or induced(dotted). The correlation coefficient analysis between individual parameters and the neural activity do not discriminate between direct and induced correlations. Canonical correlation analysis can find the hidden variables that are causing induced correlation between measured variables.

Each CCA component is a weighted sum of the original entities. To avoid having non-zero weights with small values compared to the other weights, we used sparse CCA (Witten, Tibshirani, and Hastie 2009) which enforces an adjustable penalty on the sum of the weights using LASSO (Tibshirani 1996). As a result, the number of the non-zero elements in the weight matrix will be minimized.

Results

We found CCA components between the reward model parameters (Pr_{rew} and K_{loss}) and the recorded neuronal population for 22 sessions. With 2 parameters in the reward model and more than 10 neurons in each session, we found two pairs of components in each session. Figure VIII-3 shows the scatter plot of the neural components vs. the parameter components for all trials of a sample session. The first component pair (left) is the pair with stronger correlation. The first parameter component is composed of both reward model parameters with balanced contributions. The second pair of components shows weaker correlation and the second parameter component is a mixture of both reward model parameters with opposite polarities.

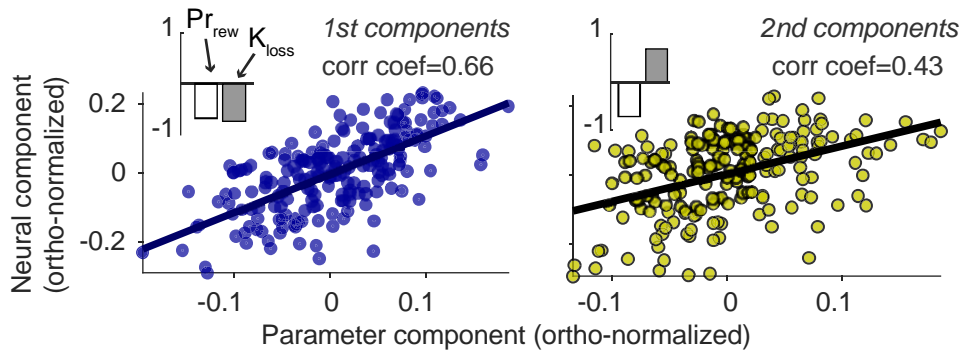


Figure VIII-3 Pairs of CCA components for a sample session. The first component (left) is the component with the strongest correlation while the second component (right) is built upon the residual of the 1st component. Insets: The weights of each reward model parameters in each component.

We observed the correlation coefficient between the component pairs is stronger than correlation between individual parameters and individual neurons. First, for the session in Figure VIII-3, we found a neuron in the population for which the absolute value of correlation with Pr_{rew} was strongest (Figure VIII-4A-left). This correlation is weaker than the correlation between parameter and neural components. Similarly, we found another neuron in the population with the strongest correlation with K_{loss} and again this correlation was weaker than the correlation among components (Figure VIII-4-right).

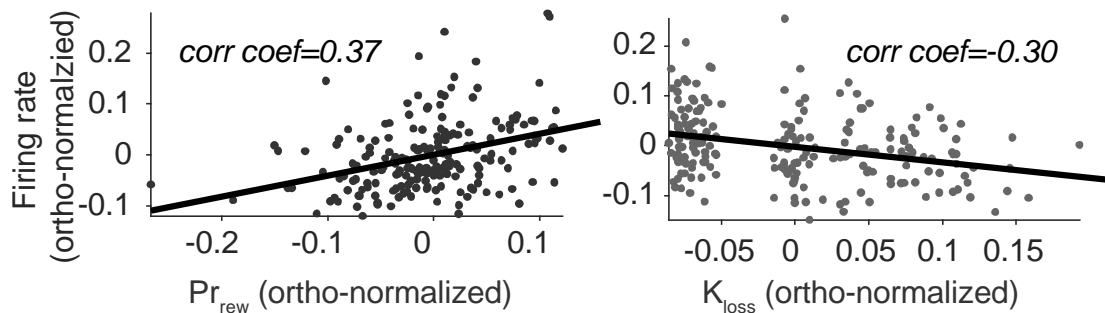


Figure VIII-4 Correlation between individual reward components (Pr_{rew} on the left and K_{loss} on the right), with pre-response activity of individual neurons for which the absolute value of the correlation was strongest compared to the rest of neurons in the population.

We observed the same trend in all sessions (Figure VIII-5). Based on this finding, we concluded that the actual parameters that are encoded in the population of dIPFC

neurons are a mixture of the reward model parameters rather than individual parameters.

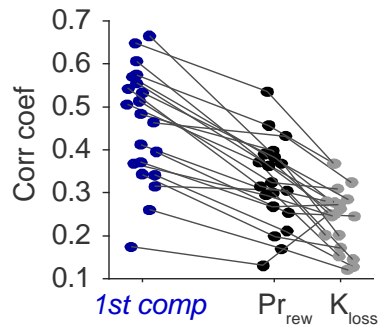


Figure VIII-5 correlation between the 1st pairs of the reward model parameter/ neural activity (blue) for each session compared to the correlation of individual parameters with the individual neuron in each session for which the absolute value of the correlation was strongest in the population.

We asked the question of whether or not the components are interpretable mixtures of the reward model parameters. We showed in CHAPTER VI that that combination of reward model parameters can predict the next action better than individual reward model parameters. When we overlapped the 1st component in the space of the reward model with the model of action prediction, we observed that this component is the discriminant of the choice (Figure VIII-6, left). We predicted the next action using the 1st component and the reward outcome and observed that the prediction performance was even better than the predictor that uses both parameters of the reward expectation model (Figure VIII-6, right, $p=0.04$ Wilcoxon signed rank test).

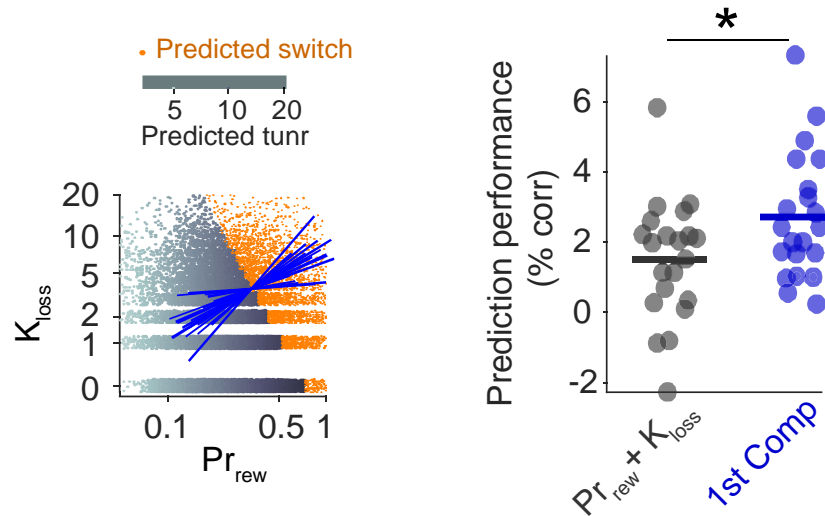


Figure VIII-6 Prediction of the next action (choice to stay vs. switch) using the 1st canonical component of population activity. Left: The orientation of the 1st component vectors in the space of the reward model parameters justify that this component is the discriminant of the stay/switch choices. Right: The performance of the choice decoder that uses the 1st component only (blue) exceeds the performance of the decoder that uses both parameters of the internal model.

Summary of results

Using Canonical Correlation Analysis, we found that the neural representation of Pr_{rew} and K_{loss} are not segregated in the neural population. The component in the neural population that has the strongest correlation with these two parameters was composed of balanced portions of both parameters. We show that this component can predict the monkey's choice (to stay on the same side or move to the other side) better than the parameters themselves. This finding suggests that the population of neurons in dlPFC that we recorded from are involved in planning the next action, consistent with previous reports that dlPFC is involved with pre-motor planning. Combined with our finding in the previous chapter, we think this area combines the information from the reward expectation with motor planning to guide the foraging strategy.

CHAPTER IX DISCUSSION AND FUTURE DIRECTIONS

Based on previous studies, we know that primates are among the most capable species in understanding the structure of the environment and they plan their actions. The fact that previous foraging experiments do not reveal fundamental differences between the foraging strategy of primates and other species might be due to a restricted experimental paradigm that limits the capacity of animals' interaction with the environment. We think our choice of free moving paradigm that allows the animal to learn the structure of the environment by freely interacting with it was crucial to our novel findings.

Here, we reported that the foraging strategy of monkeys is based on their understanding of 'rules of the game'. To our surprise, monkeys have an estimation of the probability of reward availability which was not a directly observable parameter. We think they must have come to this understanding by experimenting with the reward sources, monitoring the outcome of their actions in trial by trial basis, and integrating information over many trials. We trained regression models and observed that the next action will be predicted better than chance only if we take into the account the probability of reward availability as one of the predicting factors. We also found that we can decode this parameter from the activity of population of neurons in dlPFC.

As we explained in the introduction, we chose dlPFC to look for representation of the internal model because unlike other brain areas that represent value and reward, this area is involved in goal directed action and strategic planning. We found that the internal model parameters are represented in this area, and we can predict the next action of the animal by using components that represent these parameters. However, the components that we found do not represent the individual parameters but a mixture of them. We speculate that the internal reward model resides in other brain areas which is

directly or indirectly connected to the recorded population, so that its activity is communicated to the recorded population. Therefore, dlPFC might be receiving the information of the reward model from other brain areas, perhaps the ventro-lateral PFC (vlPFC), and then plans the next action. We have several reasons for this speculation: First, the previous studies show a great degree of similarity between dlPFC and vlPFC in reward encoding and strong connectivity between the two areas. However, the correlation of vlPFC neurons with the value of reward is slightly stronger (Kennerley and Wallis 2009). Therefore, it will not be surprising if an internal model of the task that is encoded in vlPFC is reflected in the activity of dlPFC as well. Second, dlPFC is closer to motor areas compared to vlPFC which makes it a better candidate to receive the reward expectation and plan the next motor action (Ridderinkhof et al. 2004). Third, vlPFC is involved in working memory which is required for integration of information over time to build the internal reward model (Ridderinkhof et al. 2004; Rowe and Passingham 2001). Therefore, we would expect that these two areas work together to use the internal model for strategic planning of action. Testing this hypothesis can be a promising direction for future research determining the precise role of various PFC areas in complex behavior involving continuous interactions between animals and the real world.

BIBLIOGRAPHY

- Aertsen, a M, G L Gerstein, M K Habib, and G Palm. 1989. "Dynamics of Neuronal Firing Correlation: Modulation of 'Effective Connectivity'." *Journal of Neurophysiology* 61 (5): 900–917. <http://www.ncbi.nlm.nih.gov/pubmed/2723733>.
- Aldiss, M, and M Davison. 1979. "Sensitivity of Time Allocation to Concurrent Schedule Reinforcement," no. I: 79–88.
- Alivisatos, A Paul, Miyoung Chun, George M Church, Ralph J Greenspan, Michael L Roukes, and Rafael Yuste. 2012. "The Brain Activity Map Project and the Challenge of Functional Connectomics." *Neuron*. <https://doi.org/10.1016/j.neuron.2012.06.006>.
- Alonso, J. M., W. M. Usrey, and R. C. Reid. 1996. "Precisely Correlated Firing in Cells of the Lateral Geniculate Nucleus." *Nature*. <https://doi.org/10.1038/383815a0>.
- Alonso, J M, and L M Martinez. 1998. "Functional Connectivity between Simple Cells and Complex Cells in Cat Striate Cortex." *Nature Neuroscience* 1 (5): 395–403. <https://doi.org/10.1038/1609>.
- Amemori, K.-i., S. Amemori, and a. M. Graybiel. 2015. "Motivation and Affective Judgments Differentially Recruit Neurons in the Primate Dorsolateral Prefrontal and Anterior Cingulate Cortex." *Journal of Neuroscience* 35 (5): 1939–53. <https://doi.org/10.1523/JNEUROSCI.1731-14.2015>.
- Anderson, P W. 1972. "More Is Different." *Science, New Series* 177 (4): 393–96. <http://links.jstor.org/sici?sici=0036-8075%2819720804%293%3A177%3A4047%3C393%3AMID%3E2.0.CO%3B2-N>.
- Averbeck, Bruno B., Peter E. Latham, and Alexandre Pouget. 2006. "Neural Correlations, Population Coding and Computation." *Nature Reviews Neuroscience* 7 (5): 358–66. <https://doi.org/10.1038/nrn1888>.
- Bair, W, E Zohary, and W T Newsome. 2001. "Correlated Firing in Macaque Visual Area MT: Time Scales and Relationship to Behavior." *The Journal of Neuroscience : The Official Journal of the Society for Neuroscience* 21 (5): 1676–97. <http://www.ncbi.nlm.nih.gov/pubmed/11222658>.
- Beaman, Charles B., Sarah L. Eagleman, and Valentin Dragoi. 2017. "Sensory Coding Accuracy and Perceptual Performance Are Improved during the Desynchronized Cortical State." *Nature Communications* 8 (1). Springer US: 1–14. <https://doi.org/10.1038/s41467-017-01030-4>.
- Bishop C.M. 2006. *Pattern Recognition and Machine Learning*. Edited by M. Jordan, J. Kleinberg, and B. Scholkopf. 1st ed. New York: Springer.
- Bonabeau, Eric; Dorigo, Marco; Theraulaz, Guy. 1999. "Swarm Intelligence: From Natural to Artificial Systems - Eric Bonabeau, Marco Dorigo, Guy Theraulaz - Google Books." Santa Fe Institute Studies on the Sciences of Complexity. 1999. https://books.google.com/books?id=fcTcHvSsRMYC&printsec=frontcover&source=gb_s_ge_summary_r&cad=0#v=onepage&q&f=false.

- Britten, K. H., W. T. Newsome, M. N. Shadlen, S. Celebrini, and J. A. Movshon. 2009. "A Relationship between Behavioral Choice and the Visual Responses of Neurons in Macaque MT." *Visual Neuroscience* 13 (01). Cambridge University Press: 87. <https://doi.org/10.1017/S095252380000715X>.
- Cohen, Marlene R, and Adam Kohn. 2011. "Measuring and Interpreting Neuronal Correlations." *Nature Neuroscience* 14 (7): 811–19. <https://doi.org/10.1038/nn.2842>.
- Cohen MR, and Maunsell JHR. 2009. "Attention Improves Performance Primarily by Reducing Interneuronal Correlations." *Nature Neuroscience* 12: 1594–1601. <https://doi.org/10.1038/nn.2439>.
- Crick, Francis, and Christof Koch. 1998. "Constraints on Cortical and Thalamic Projections: The No-Strong-Loops Hypothesis." *Nature* 391 (6664): 245–50. <https://doi.org/10.1038/34584>.
- Cunningham, John P, and Byron M Yu. 2014. "Dimensionality Reduction for Large-Scale Neural Recordings." *Nature Neuroscience* 17 (11): 1500–1509. <https://doi.org/10.1038/nn.3776>.
- Dan, Y, J J Atick, and R C Reid. 1996. "Efficient Coding of Natural Scenes in the Lateral Geniculate Nucleus: Experimental Test of a Computational Theory." *The Journal of Neuroscience : The Official Journal of the Society for Neuroscience* 16 (10): 3351–62. <http://www.ncbi.nlm.nih.gov/pubmed/8627371>.
- Engbert, Ralf, and Reinhold Kliegl. 2003. "Microsaccades Uncover the Orientation of Covert Attention." *Vision Research* 43 (9): 1035–45. [https://doi.org/10.1016/S0042-6989\(03\)00084-1](https://doi.org/10.1016/S0042-6989(03)00084-1).
- Felleman, D J, and D C Van Essen. "Distributed Hierarchical Processing in the Primate Cerebral Cortex." *Cerebral Cortex (New York, N.Y. : 1991)* 1 (1): 1–47. <http://www.ncbi.nlm.nih.gov/pubmed/1822724>.
- Fries, Pascal. 2005. "A Mechanism for Cognitive Dynamics: Neuronal Communication through Neuronal Coherence." *Trends in Cognitive Sciences* 9 (10): 474–80. <https://doi.org/10.1016/j.tics.2005.08.011>.
- Gibbon, J, R M Church, S Fairhurst, and a Kacelnik. 1988. "Scalar Expectancy Theory and Choice between Delayed Rewards." *Psychological Review* 95 (1): 102–14. <https://doi.org/10.1037/0033-295X.95.1.102>.
- Gilbert, Charles D, and Wu Li. 2013. "Top-down Influences on Visual Processing." *Nature Reviews. Neuroscience* 14 (5): 350–63. <https://doi.org/10.1038/nrn3476>.
- Gollisch, Tim, and Markus Meister. 2008. "Rapid Neural Coding in the Retina with Relative Spike Latencies." *Science* 319. <http://science.sciencemag.org/content/319/5866/1108/tab-pdf>.
- Goodfellow, Ian, Yoshua Bengio, and Aaron Courville. 2016. "Deep Learning." The MIT Press. 2016. <https://books.google.com/books?id=Np9SDQAAQBAJ&printsec=frontcover&dq=deep+learning&hl=en&sa=X&ved=0ahUKEWjuyrjGk73bAhUEUK0KHdp5D0cQ6AEIKTAA#v=onepage&q=deep+learning&f=false>.
- Hansen, Bryan J, and Valentin Dragoi. 2011. "Adaptation-Induced Synchronization in

- Laminar Cortical Circuits." <https://doi.org/10.1073/pnas.1102017108/-/DCSupplemental.www.pnas.org/cgi/doi/10.1073/pnas.1102017108>.
- Herrnstein, Richard J., Howard Rachlin, and David I. Laibson. 1997. *The Matching Law : Papers in Psychology and Economics*. Russell Sage Foundation.
<https://books.google.com/books?id=08msDavsucYC&pg=PA3&dq=melioration+matching+law+economics&hl=en&sa=X&ved=0ahUKEwiNx9D7473bAhXCz1MKHVEIAskQ6AEIKTAA#v=onepage&q=melioration+matching+law+economics&f=false>.
- Hirabayashi, Toshiyuki, and Yasushi Miyashita. 2005. "Dynamically Modulated Spike Correlation in Monkey Inferior Temporal Cortex Depending on the Feature Configuration within a Whole Object." *The Journal of Neuroscience : The Official Journal of the Society for Neuroscience* 25 (44): 10299–307.
<https://doi.org/10.1523/JNEUROSCI.3036-05.2005>.
- Histed, Mark H, and John H R Maunsell. 2013. "Cortical Neural Populations Can Guide Behavior by Integrating Inputs Linearly , Independent of Synchrony" 2013.
<https://doi.org/10.1073/pnas.1318750111/-/DCSupplemental.www.pnas.org/cgi/doi/10.1073/pnas.1318750111>.
- Kennerley, S W, and J D Wallis. 2009. "Reward-Dependent Modulation of Working Memory in Lateral Prefrontal Cortex." *Journal of Neuroscience* 29 (10): 3259–70.
<https://doi.org/Doi+10.1523/Jneurosci.5353-08.2009>.
- Kobak, Dmitry, Wieland Brendel, Christos Constantinidis, Claudia E Feierstein, Adam Kepecs, Zachary F Mainen, Ranulfo Romo, Xue-lian Qi, Naoshige Uchida, and Christian K Machens. 2016. "Demixed Principal Component Analysis of Neural Population Data." *ELife* 5: 1–37. <https://doi.org/10.7554/eLife.10989>.
- König, P, A K Engel, and W Singer. 1996. "Integrator or Coincidence Detector? The Role of the Cortical Neuron Revisited." *Trends in Neurosciences* 19 (4): 130–37.
<http://www.ncbi.nlm.nih.gov/pubmed/8658595>.
- Lamme, Victor A.F., Hans Supèr, and Henk Spekreijse. 1998. "Feedforward, Horizontal, and Feedback Processing in the Visual Cortex." *Current Opinion in Neurobiology* 8 (4): 529–35. [https://doi.org/10.1016/S0959-4388\(98\)80042-1](https://doi.org/10.1016/S0959-4388(98)80042-1).
- Larkum, Matthew. 2013. "A Cellular Mechanism for Cortical Associations: An Organizing Principle for the Cerebral Cortex." *Trends in Neurosciences* 36 (3). Elsevier Ltd: 141–51.
<https://doi.org/10.1016/j.tins.2012.11.006>.
- Leonard, Carly J, Steven J Luck, Matthew T Schmolesky, Youngchang Wang, Doug P Hanes, Kirk G Thompson, Stefan Leutgeb, Jeffrey D Schall, and Audie G Leventhal. 2011. "Signal Timing Across the Macaque Visual System Signal Timing Across the Macaque Visual System," 3272–78.
- Markram, Henry. 2006. "The Blue Brain Project." *Nature Reviews* 7: 153–60.
<https://www.nature.com/articles/nrn1848.pdf>.
- McAdams, Carrie J., and John H.R. Maunsell. 1999. "Effects of Attention on the Reliability of Individual Neurons in Monkey Visual Cortex." *Neuron* 23 (4): 765–73.
[https://doi.org/10.1016/S0896-6273\(01\)80034-9](https://doi.org/10.1016/S0896-6273(01)80034-9).
- Mcginley, Matthew J, Stephen V David, and David A McCormick. 2015. "Cortical Membrane

- Potential Signature of Optimal States for Sensory Signal Detection." *Neuron* 87: 179–92. <https://doi.org/10.1016/j.neuron.2015.05.038>.
- Meister, Markus, Leon Lagnado, and Denis A Baylor. 1995. "Concerted Signaling by Retinal Ganglion Cells." *Source: Science, New Series* 270 (17): 1207–10. <http://www.jstor.org/stable/2889227>.
- Mitchell, Jude F, Kristy a Sundberg, and John H Reynolds. 2009. "Spatial Attention Decorrelates Intrinsic Activity Fluctuations in Macaque Area V4." *Neuron* 63 (6). Elsevier Ltd: 879–88. <https://doi.org/10.1016/j.neuron.2009.09.013>.
- Nienborg, H., and B. G. Cumming. 2006. "Macaque V2 Neurons, But Not V1 Neurons, Show Choice-Related Activity." *Journal of Neuroscience* 26 (37): 9567–78. <https://doi.org/10.1523/JNEUROSCI.2256-06.2006>.
- Okun, M., P. Yger, S. L. Marguet, F. Gerard-Mercier, A. Benucci, S. Katzner, L. Busse, M. Carandini, and K. D. Harris. 2012. "Population Rate Dynamics and Multineuron Firing Patterns in Sensory Cortex." *Journal of Neuroscience* 32 (48): 17108–19. <https://doi.org/10.1523/JNEUROSCI.1831-12.2012>.
- Patterson, Dan W. 1996. *Artificial Neural Networks : Theory and Applications*. Prentice Hall. https://books.google.com/books/about/Artificial_Neural_Networks.html?id=tJokAQA AIAAJ.
- Pipa, Gordon, Diek W Wheeler, Wolf Singer, and Danko Nikolić. 2008. "NeuroXidence: Reliable and Efficient Analysis of an Excess or Deficiency of Joint-Spike Events." *Journal of Computational Neuroscience* 25 (1): 64–88. <https://doi.org/10.1007/s10827-007-0065-3>.
- Purushothaman, Gopathy, and David C Bradley. 2005. "Neural Population Code for Fine Perceptual Decisions in Area MT." *Nature Neuroscience* 8 (1): 99–106. <https://doi.org/10.1038/nn1373>.
- Ramkumar, Pavan, Brian Dekleva, Sam Cooler, Lee Miller, and Konrad Kording. 2016. "Premotor and Motor Cortices Encode Reward." *PLoS ONE* 11 (8). <https://doi.org/10.1371/journal.pone.0160851>.
- Reynolds, John H, and Leonardo Chelazzi. 2004. "Attentional Modulation of Visual Processing." *Annu. Rev. Neurosci* 27: 611–47. <https://doi.org/10.1146/annurev.neuro.26.041002.131039>.
- Ridderinkhof, K Richard, Wery P M Van Den Wildenberg, Sidney J Segalowitz, and Cameron S Carter. 2004. "Neurocognitive Mechanisms of Cognitive Control: The Role of Prefrontal Cortex in Action Selection, Response Inhibition, Performance Monitoring, and Reward-Based Learning." *Brain and Cognition* 56 56: 129–40. <https://doi.org/10.1016/j.bandc.2004.09.016>.
- Riehle, a. 1997. "Spike Synchronization and Rate Modulation Differentially Involved in Motor Cortical Function." *Science* 278 (5345): 1950–53. <https://doi.org/10.1126/science.278.5345.1950>.
- Rowe, James B, and Richard E Passingham. 2001. "Working Memory for Location and Time: Activity in Prefrontal Area 46 Relates to Selection Rather than Maintenance in Memory." *NeuroImage* 14 (1 I): 77–86. <https://doi.org/10.1006/nimg.2001.0784>.

- Schneider, Susan M, and Michael Davison. 2005. "Demarcated Response Sequences and Generalised Matching." *Behavioural Processes* 70 (1): 51–61.
<https://doi.org/10.1016/j.beproc.2005.04.005>.
- Schultz, Wolfram. n.d. "Predictive Reward Signal of Dopamine Neurons." Accessed June 6, 2018. <https://www.physiology.org/doi/pdf/10.1152/jn.1998.80.1.1>.
- Shadlen, M N, and J a Movshon. 1999. "Synchrony Unbound: A Critical Evaluation of the Temporal Binding Hypothesis." *Neuron* 24 (1): 67–77, 111–25.
<http://www.ncbi.nlm.nih.gov/pubmed/10677027>.
- Shull, Richard L., and Stanley S. Pliskoff. 1967. "Changeover Delay and Concurrent Schedules: Some Effects on Relative Performance Measures1." *Journal of the Experimental Analysis of Behavior* 10 (6): 517–27.
<https://doi.org/10.1901/jeab.1967.10-517>.
- Smith, John M. 1982. "Evolution and the Theory of Games." Cambridge University. 1982.
https://books.google.com/books/about/Evolution_and_the_Theory_of_Games.html?id=Nag2IhmPS3gC&printsec=frontcover&source=kp_read_button#v=onepage&q&f=false.
- Smith, Matthew a, Xiaoxuan Jia, Amin Zandvakili, and Adam Kohn. 2012. "Laminar Dependence of Neuronal Correlations in Visual Cortex." *Journal of Neurophysiology* 109 (4): 940–47. <https://doi.org/10.1152/jn.00846.2012>.
- Smolyanskaya, Alexandra, Ralf M. Haefner, Stephen G. Lomber, and Richard T. Born. 2015. "A Modality-Specific Feedforward Component of Choice-Related Activity in MT." *Neuron* 87 (1). Elsevier Inc.: 208–19. <https://doi.org/10.1016/j.neuron.2015.06.018>.
- Strang, Gilbert. 2016. *Linear Algebra and Its Applications*.
https://books.google.com/books?id=9A7jBQAAQBAJ&source=gbs_similarbooks.
- Sugrue, Leo P., Greg S. Corrado, and William T. Newsome. 2004. "Matching Behavior and the Representation of Value in the Parietal Cortex" 304 (October): 457–61.
- Takeuchi, Daigo, Toshiyuki Hirabayashi, Keita Tamura, and Yasushi Miyashita. 2011a. "Reversal of Interlaminar Signal between Sensory and Memory Processing in Monkey Temporal Cortex_SUP." *Science (New York, N.Y.)* 331 (6023): 1443–47.
<https://doi.org/10.1126/science.1199967>.
- Thorndike, Robert M. 2000. "Canonical Correlation Analysis." In *Handbook of Applied Multivariate Statistics and Mathematical Modeling*, 237–63. Elsevier.
<https://doi.org/10.1016/B978-012691360-6/50010-0>.
- Tibshirani, Robert. 1996. "Regression Shrinkage and Selection via the Lasso." *J. R. Statist. Soc. B* 58 (1): 267–88.
<https://www.jstor.org/stable/pdf/2346178.pdf?refreqid=excelsior%3Aa5cd80e7f90a8239796308971b0b0b37>.
- Torre, Emiliano, David Picado-Muiño, Michael Denker, Christian Borgelt, and Sonja Grün. 2013. "Statistical Evaluation of Synchronous Spike Patterns Extracted by Frequent Item Set Mining." *Frontiers in Computational Neuroscience* 7 (October): 132.
<https://doi.org/10.3389/fncom.2013.00132>.
- Torre, Emiliano, Pietro Quaglio, Michael Denker, Thomas Brochier, Alexa Riehle, and Sonja

- Grün. 2016. "Synchronous Spike Patterns in Macaque Motor Cortex during an Instructed-Delay Reach-to-Grasp Task." *The Journal of Neuroscience: The Official Journal of the Society for Neuroscience* 36 (32): 8329–40. <https://doi.org/10.1523/JNEUROSCI.4375-15.2016>.
- Uka, T., S. Tanabe, M Watabane, and I Fujita. 2005. "Neural Correlates of Fine Depth Discrimination in Monkey Inferior Temporal Cortex." *Journal of Neuroscience* 25 (46): 10796–802. <https://doi.org/10.1523/JNEUROSCI.1637-05.2005>.
- Ungerleider, Leslie G, Thelma W Galkin, Robert Desimone, and Ricardo Gattass. 2008. "Cortical Connections of Area V4 in the Macaque." *Cerebral Cortex (New York, N.Y. : 1991)* 18 (3): 477–99. <http://cercor.oxfordjournals.org/content/18/3/477.long>.
- Vaadia, E., I. Haalman, M. Abeles, H. Bergman, Y. Prut, H. Slovin, and A. Aertsen. 1995. "Dynamics of Neuronal Interactions in Monkey Cortex in Relation to Behavioural Events." *Nature* 373 (6514). Nature Publishing Group: 515–18. <https://doi.org/10.1038/373515a0>.
- Witten, Daniela M, Robert Tibshirani, and Trevor Hastie. 2009. "A Penalized Matrix Decomposition, with Applications to Sparse Principal Components and Canonical Correlation Analysis." *Biostatistics* 10 (3): 515–34. <https://doi.org/10.1093/biostatistics/kxp008>.
- Yin, Ming, David a Borton, Jacob Komar, Naubahar Agha, Yao Lu, Hao Li, Jean Laurens, et al. 2014. "Wireless Neurosensor for Full-Spectrum Electrophysiology Recordings during Free Behavior." *Neuron* 84 (6): 1170–82. <https://doi.org/10.1016/j.neuron.2014.11.010>.
- Yin, Ming, Member Ieee, Hao Li, Christopher Bull, David A Borton, Student Member, Aceros Member Ieee, Lawrence Larson, and Arto V Nurmikko. 2013. "An Externally Head-Mounted Wireless Neural Recording Device for Laboratory Animal Research and Possible Human Clinical Use," 3–7.
- Zandvakili, Amin, and Adam Kohn. 2015. "Coordinated Neuronal Activity Enhances Corticocortical Communication." *Neuron* 87 (4). Elsevier Inc.: 827–39. <https://doi.org/10.1016/j.neuron.2015.07.026>.
- Zohary, E, MN Shadlen, and WT Newsome. 1994. "Correlated Neuronal Discharge Rate and Its Implications for Psychophysical Performance." <http://www.nature.com/nature/journal/v370/n6485/abs/370140a0.html>.

*“After sleeping through a hundred million centuries
We have finally opened our eyes on a sumptuous planet,
sparkling with color, bountiful with life
Within decades we must close our eyes again
Isn't it a noble and enlightened way of spending our brief time in the sun
To work at understanding the universe and how we have come to wake up in it?”*

This is how I answer when I am asked—as I am surprisingly often—why I bother to get up in the mornings.”

— Richard Dawkins